1–333)-stimulated GTPase activity, GDP bound to HRAS and RRAS proteins was exchanged with excess mantGTP in the presence of alkaline phosphatase. Unbound nucleotides were removed by NAP5 column, and the RAS/mantGTP proteins were snap-frozen in liquid nitrogen (66). GAP-stimulated GTP hydrolysis of RAS proteins (0.2 μM) was measured in 30 mM Tris–HCl, pH 7.5, 10 mM $MgCl_2$, 3 mM DTE at 25°C using a Hightech TgK Scientific stopped-flow instrument. Reactions measured the decrease in fluorescence owing to hydrolysis of mantGTP. This decay was fit by a single exponential.

Effector binding assays were performed in 30 mM Tris–HCl, pH 7.5, 100 mM NaCl, 5 mM $MgCl_2$, 3 mM DTE at 25°C using a Fluoromax 4 fluorimeter in polarization mode. Increasing amounts of GST-tagged RAS-binding domains (RBD) of RAS effectors were titrated to 0.3 μM mantGppNHp-bound RAS proteins resulting in an increase of polarization (64). The dissociation constants (K_d) were calculated by fitting the concentration-dependent binding curve using a quadratic ligand binding equation.

For cell-based assays, COS-7 cells were transiently transfected with FLAG-tagged $RRAS^{WT}$, $RRAS^{V55M}$ or $RRAS^{G39dup}$ by the DEAE-dextran method. For serum conditions, cells were incubated for 48 h in 10% FCS. In serum-starved conditions, serum was changed to basal medium midway between the transfection and harvesting. Transfected COS-7 cells were harvested and lysed in fishing buffer [50 mM Tris–HCl, pH 7.5, 2 mM $MgCl_2$, 100 mM NaCl, 1% IGEPAL CA-630, 10% glycerol, EDTA-free protease inhibitor cocktail (Roche, 1 tablet/50 ml buffer), 20 mM disodium β-glycerol phosphate and 1 mM Na_3VO_4]. Cleared cell lysates were incubated with GSH-beads loaded with GST-RAF1-RBD. GTP-bound proteins and total recombinant proteins were analysed by immunoblotting with anti-FLAG antibody. Antibodies against MEK1/2, ERK1/2, AKT, phospho-MEK1/2 (Ser217/221), phospho-ERK1/2 (Thr202/Tyr204) and phospho-AKT (Thr308) were purchased from Cell Signaling Technology (68).

Caenorhabditis elegans studies

Culture and maintenance of animals were as previously described (69). The *let-60(n1046)* (*let-60/RAS* gain-of-function allele) and *let-23(sy1)* (*let-23/EGFR* hypomorphic allele) strains were provided by the *Caenorhabditis Genetics Center* (University of Minnesota). The three-nucleotide insertion, c.81_82insGGC ($ras\text{-}1^{G27dup}$), corresponding to c.116_118dup in *RRAS*, was introduced in the wild-type cDNA ($ras\text{-}1^{WT}$) (*C. elegans* ORF clone AAB03320, Thermo Scientific) by site-directed mutagenesis (QuikChange Site-Directed Mutagenesis Kit, Stratagene). *ras-1* cDNAs were subcloned into the pPD49.83 heat shock-inducible vector (a gift of A. Fire, Stanford University School of Medicine). Germline transformation was performed as described (70). pJM371 plasmid [*pelt-2*::NLS::*RFP*] (a gift from J.D. McGhee, University of Calgary), which drives red fluorescent protein (RFP) expression in intestinal cell nuclei, was used as co-injection marker (30 ng/μl). Two different doses of constructs were injected (30 and 100 ng/μl). Animals from at least three independent transgenic lines for each construct and each dose of injection (i.e. six lines expressing $ras\text{-}1^{WT}$ and six lines expressing $ras\text{-}1^{G27dup}$) were heat-shocked in parallel and scored blindly at a Leica MZ10F dissecting microscope to check for the presence of protruding vulvae (Pvl phenotype) and multiple ectopic pseudovulvae (Muv phenotype), count the number of eggs retained in the uterus (Egl phenotype) and identify animals that had become bag-of-worms (Bag phenotype). Isogenic worms that had lost the transgene were cloned separately and used as controls. Following heat shock, all the transgenic lines expressing $ras\text{-}1^{WT}$ or $ras\text{-}1^{G27dup}$ showed a variable degree of these phenotypes. Lines *gbEx555a*[*hsp-16.41*::$ras\text{-}1^{WT}$;*pelt-2*::NLS::*RFP*] and *gbEx557a*[*hsp-16.41*::$ras\text{-}1^{G27dup}$;*pelt-2*::NLS::*RFP*] were scored quantitatively in triplicate experiments at the compound microscope and used for further analyses. Genetic crosses were performed according to standard methods (69). The genotype of individual alleles was confirmed by direct sequencing of the appropriate genomic region. After each cross, isogenic worms that had lost the transgene were used as controls.

To investigate VPCs induction and vulva morphogenesis, synchronized hermaphrodites carrying each transgene and the corresponding isogenic controls were heat-shocked in parallel at early L3 stage (33°C, 1 h, followed by 30°C, 1 h). Animals were scored at the compound microscope for vulval induction at late L3 and L4 stages, and for Pvl/Egl/Bag phenotypes at the adult stage. Microscopy observations were performed with a Nikon Eclipse 80i instrument equipped with Nomarski differential interference contrast optics on live animals mounted on 2% agarose pads containing 10 mM sodium azide as anaesthetic.

SUPPLEMENTARY MATERIAL

Supplementary Material is available at *HMG* online.

ACKNOWLEDGEMENTS

We are grateful to the participating patients and their families. We thank Serenella Venanzi (Istituto Superiore di Sanità, Rome, Italy), Michela Bonaguro (Policlinico S.Orsola-Malpighi, Bologna, Italy), Federica Consoli (Istituto Mendel, Rome, Italy) and Cédric Vignal and Sabrina Pereira (Hôpital Robert Debré, Paris, France) for skilful technical assistance, and the Open Laboratory (IGB-CNR, Naples, Italy) for experimental support. We also thank Paolo Bazzicalupo (IGB-CNR) for critical reading of the manuscript, paediatricians from the *Société Française des Cancers de l'Enfant* (SFCE) for providing biological material from their patients and CINECA for computational resources. Some nematode strains used in this work were provided by the *Caenorhabditis Genetics Center* (University of Minnesota, Minneapolis, MN, USA) funded by the NIH Office of Research Infrastructure Programs (P40OD010440).

Conflict of Interest statement. None declared.

FUNDING

This work was supported by grants from the ERA-Net for research programmes on rare diseases 2009 (NSEuroNet to M.Z., H.C., M.R.A. and M.T.), Telethon-Italy (GGP10020 and GGP13107 to M.T.), AIRC (IG 13360 to M.T.), NGFNplus program of the German Ministry of Science and Education (01GS08100 to M.R.A.), German Research Foundation through the Collaborative Research Center 974 (Communication and Systems Relevance

during Liver Injury and Regeneration to M.R.A.) and NIH (HL071207 to B.D.G.). F.P. was recipient of a research fellowship from '*Associazione Italiana Sindromi di Costello e cardiofaciocutanea*'. Funding to pay the Open Access publication charges for this article was provided by Telethon-Italy.

REFERENCES

1. Mitin, N., Rossman, K.L. and Der, C.J. (2005) Signaling interplay in Ras superfamily function. *Curr. Biol.*, **15**, R563–R574.
2. Mendoza, M.C., Er, E.E. and Blenis, J. (2011) The Ras-ERK and PI3K-mTOR pathways: cross-talk and compensation. *Trends Biochem. Sci.*, **36**, 320–328.
3. Harris, T.J.R. and McCormick, F. (2010) The molecular pathology of cancer. *Nat. Rev. Clin. Oncol.*, **7**, 251–265.
4. Pylayeva-Gupta, Y., Grabocka, E. and Bar-Sagi, D. (2011) RAS oncogenes: weaving a tumorigenic web. *Nat. Rev. Cancer*, **11**, 761–774.
5. Roberts, A.E., Allanson, J.E., Tartaglia, M. and Gelb, B.D. (2013) Noonan syndrome. *Lancet*, **381**, 333–342.
6. Schubbert, S., Shannon, K. and Bollag, G. (2007) Hyperactive Ras in developmental disorders and cancer. *Nat. Rev. Cancer*, **7**, 295–308.
7. Tartaglia, M. and Gelb, B.D. (2010) Disorders of dysregulated signal traffic through the RAS-MAPK pathway: phenotypic spectrum and molecular mechanisms. *Ann. N. Y. Acad. Sci.*, **1214**, 99–121.
8. Rauen, K.A. (2013) The RASopathies. *Annu. Rev. Genomics Hum. Genet.*, **14**, 355–369.
9. Aoki, Y., Niihori, T., Banjo, T., Okamoto, N., Mizuno, S., Kurosawa, K., Ogata, T., Takada, F., Yano, M., Ando, T. *et al.* (2013) Gain-of-function mutations in RIT1 cause Noonan syndrome, a RAS/MAPK pathway syndrome. *Am. J. Hum. Genet.*, **93**, 173–180.
10. Tartaglia, M., Gelb, B.D. and Zenker, M. (2011) Noonan syndrome and clinically related disorders. *Best Pract. Res. Clin. Endocrinol. Metab.*, **25**, 161–179.
11. Kratz, C.P., Rapisuwon, S., Reed, H., Hasle, H. and Rosenberg, P.S. (2011) Cancer in Noonan, Costello, cardiofaciocutaneous and LEOPARD syndromes. *Am. J. Med. Genet. C Semin. Med. Genet.*, **157C**, 83–89.
12. Gripp, K.W. (2005) Tumor predisposition in Costello syndrome. *Am. J. Med. Genet. C Semin. Med. Genet.*, **137C**, 72–77.
13. Loh, M.L. (2011) Recent advances in the pathogenesis and treatment of juvenile myelomonocytic leukaemia. *Br. J. Haematol.*, **152**, 677–687.
14. McKay, M.M. and Morrison, D.K. (2007) Integrating signals from RTKs to ERK/MAPK. *Oncogene*, **26**, 3113–3121.
15. Dannenfelser, R., Clark, N.R. and Ma'ayan, A. (2012) Genes2FANs: connecting genes through functional association networks. *BMC Bioinformatics*, **13**, 156.
16. Lowe, D.G., Capon, D.J., Delwart, E., Sakaguchi, A.Y., Naylor, S.L. and Goeddel, D.V. (1987) Structure of the human and murine R-ras genes, novel genes closely related to ras proto-oncogenes. *Cell*, **48**, 137–146.
17. Wennerberg, K., Rossman, K.L. and Der, C.J. (2005) The Ras superfamily at a glance. *J. Cell Sci.*, **118**, 843–846.
18. Krengel, U., Schlichting, I., Scherer, A., Schumann, R., Frech, M., John, J., Kabsch, W., Pai, E.F. and Wittinghofer, A. (1990) Three-dimensional structures of H-ras p21 mutants: molecular basis for their inability to function as signal switch molecules. *Cell*, **62**, 539–548.
19. Saez, R., Chan, A.M., Miki, T. and Aaronson, S.A. (1994) Oncogenic activation of human R-ras by point mutations analogous to those of prototype H-ras oncogenes. *Oncogene*, **9**, 2977–2982.
20. Aoki, Y., Niihori, T., Kawame, H., Kurosawa, K., Ohashi, H., Tanaka, Y., Filocamo, M., Kato, K., Suzuki, Y., Kure, S. *et al.* (2005) Germline mutations in HRAS proto-oncogene cause Costello syndrome. *Nat. Genet.*, **37**, 1038–1040.
21. Bollag, G., Adler, F., elMasry, N., McCabe, P.C., Conner, E. Jr, Thompson, P., McCormick, F. and Shannon, K. (1996) Biochemical characterization of a novel KRAS insertion mutation from a human leukemia. *J. Biol. Chem.*, **271**, 32491–32494.
22. Reimann, C., Arola, M., Bierings, M., Karow, A., van den Heuvel-Eibrink, M.M., Hasle, H., Niemeyer, C.M. and Kratz, C.P. (2006) A novel somatic K-Ras mutation in juvenile myelomonocytic leukemia. *Leukaemia*, **20**, 1637–1638.
23. Murugan, A.K., Hong, N.T., Cuc, T.T., Hung, N.C., Munirajan, A.K., Ikeda, M.A. and Tsuchida, N. (2009) Detection of two novel mutations and relatively high incidence of H-RAS mutations in Vietnamese oral cancer. *Oral. Oncol.*, **45**, e161–e166.
24. Sartori, G., Cavazza, A., Sgambato, A., Marchioni, A., Barbieri, F., Longo, L., Bavieri, M., Murer, B., Meschiari, E., Tamberi, S. *et al.* (2009) EGFR and K-ras mutations along the spectrum of pulmonary epithelial tumors of the lung and elaboration of a combined clinicopathologic and molecular scoring system to predict clinical responsiveness to EGFR inhibitors. *Am. J. Clin. Pathol.*, **131**, 478–489.
25. Milburn, M.V., Tong, L., deVos, A.M., Brünger, A., Yamaizumi, Z., Nishimura, S. and Kim, S.-H. (1990) Molecular switch for signal transduction: structural differences between active and inactive forms of protooncogenic ras proteins. *Science*, **247**, 939–945.
26. Diaz, J.F., Wroblowski, B., Schlitter, J. and Engelborghs, Y. (1997) Calculation of pathways for the conformational transition between the GTP- and GDP-bound states of the Ha-ras-p21 protein: calculations with explicit solvent simulations and comparison with calculations in vacuum. *Proteins*, **28**, 434–451.
27. Kuppens, S., Díaz, J.F. and Engelborghs, Y. (1999) Characterization of the hinges of the effector loop in the reaction pathway of the activation of ras-proteins. Kinetics of binding of beryllium trifluoride to V29G and I36G mutants of Ha-ras-p21. *Prot. Sci.*, **8**, 1860–1866.
28. Ma, J. and Karplus, M. (1997) Molecular switch in signal transduction: reaction paths of the conformational changes in ras p21. *Proc. Natl. Acad. Sci. USA*, **94**, 11905–11910.
29. Gorfe, A.A., Grant, B.J. and McCammon, J.A. (2008) Mapping the nucleotide and isoform-dependent structural and dynamical features of Ras proteins. *Structure*, **16**, 885–896.
30. Hall, B.E., Yang, S.S., Boriack-Sjodin, P.A., Kuriyan, J. and Bar-Sagi, D. (2001) Structure-based mutagenesis reveals distinct functions for Ras switch 1 and switch 2 in Sos-catalyzed guanine nucleotide exchange. *J. Biol. Chem.*, **276**, 27629–27637.
31. Suzuki, J., Kaziro, Y. and Koide, H. (1997) An activated mutant of R-Ras inhibits cell death caused by cytokine deprivation in BaF3 cells in the presence of IGF-I. *Oncogene*, **15**, 1689–1697.
32. Scheffzek, K., Ahmadian, M.R., Kabsch, W., Wiesmüller, L., Lautwein, A., Schmitz, F. and Wittinghofer, A. (1997) The Ras-RasGAP complex: structural basis for GTPase activation and its loss in oncogenic Ras mutants. *Science*, **277**, 333–338.
33. Lundquist, E.A. (2006) Small GTPases. In *WormBook*. The *C. elegans* Research Community, WormBook (ed.), http://www.wormbook.org. doi:/10.1895/wormbook.1.67.1.
34. Sternberg, P.W. (2005) Vulval development. In *Wormbook*. The *C. elegans* Research Community (ed.), http://www.wormbook.org. doi:10.1895/wormbook.1.6.1.
35. Sundaram, M.V. (2006) RTK/Ras/MAPK signaling. In *Wormbook*. The *C. elegans* Research Community (ed.), http://www.wormbook.org. doi/10.1895/wormbook.1.80.1.
36. Eisenmann, D.M. and Kim, S.K. (2000) Protruding vulva mutants identify novel loci and Wnt signaling factors that function during *Caenorhabditis elegans* vulva development. *Genetics*, **156**, 1097–1116.
37. Kishore, R.S. and Sundaram, M.V. (2002) ced-10 Rac and mig-2 function redundantly and act with unc-73 trio to control the orientation of vulval cell divisions and migrations in *Caenorhabditis elegans*. *Dev. Biol.*, **241**, 339–348.
38. Cordeddu, V., Di Schiavi, E., Pennacchio, L.A., Ma'ayan, A., Sarkozy, A., Fodale, V., Cecchetti, S., Cardinale, A., Martin, J., Schackwitz, W. *et al.* (2009) Mutation of SHOC2 promotes aberrant protein N-myristoylation and causes Noonan-like syndrome with loose anagen hair. *Nat. Genet.*, **41**, 1022–1026.
39. Cox, A.D., Brtva, T.R., Lowe, D.G. and Der, C.J. (1994) R-Ras induces malignant, but not morphologic, transformation of NIH3T3 cells. *Oncogene*, **9**, 3281–3288.
40. Wozniak, M.A., Kwong, L., Chodniewicz, D., Klemke, R.L. and Keely, P.J. (2005) R-Ras controls membrane protrusion and cell migration through the spatial regulation of Rac and Rho. *Mol. Biol. Cell*, **16**, 84–96.
41. Osada, M., Tolkacheva, T., Li, W., Chan, T.O., Tsichlis, P.N., Saez, R., Kimmelman, A.C. and Chan, A.M. (1999) Differential roles of Akt, Rac, and Ral in R-Ras-mediated cellular transformation, adhesion, and survival. *Mol. Cell. Biol.*, **19**, 6333–6344.
42. Marte, B.M., Rodriguez-Viciana, P., Wennström, S., Warne, P.H. and Downward, J. (1997) R-Ras can activate the phosphoinositide 3-kinase but not the MAP kinase arm of the Ras effector pathways. *Curr. Biol.*, **7**, 63–70.

43. Jopling, C., van Geemen, D. and den Hertog, J. (2007) Shp2 knockdown and Noonan/LEOPARD mutant Shp2-induced gastrulation defects. *PLoS Genet.*, **3**, e225.
44. Wang, S., Yu, W.M., Zhang, W., McCrae, K.R., Neel, B.G. and Qu, C.K. (2009) Noonan syndrome/leukemia-associated gain-of-function mutations in SHP-2 phosphatase (PTPN11) enhance cell migration and angiogenesis. *J. Biol. Chem.*, **284**, 913–920.
45. Chen, P.C., Wakimoto, H., Conner, D., Araki, T., Yuan, T., Roberts, A., Seidman, C., Bronson, R., Neel, B., Seidman, J.G. *et al.* (2010) Activation of multiple signalling pathways causes developmental defects in mice with a Noonan syndrome-associated Sos1 mutation. *J. Clin. Invest.*, **120**, 4353–4365.
46. Emanuel, P.D. (2008) Juvenile myelomonocytic leukemia and chronic myelomonocytic leukemia. *Leukemia*, **22**, 1335–1342.
47. Niemeyer, C.M. and Kratz, C.P. (2008) Paediatric myelodysplastic syndromes and juvenile myelomonocytic leukaemia: molecular classification and treatment options. *Br. J. Haematol.*, **140**, 610–624.
48. Matsuda, K., Shimada, A., Yoshida, N., Ogawa, A., Watanabe, A., Yajima, S., Iizuka, S., Koike, K., Yanai, F., Kawasaki, K. *et al.* (2007) Spontaneous improvement of hematologic abnormalities in patients having juvenile myelomonocytic leukemia with specific RAS mutations. *Blood*, **109**, 5477–5480.
49. Flotho, C., Kratz, C.P., Bergsträsser, E., Hasle, H., Starý, J., Trebo, M., van den Heuvel-Eibrink, M.M., Wójcik, D., Zecca, M., Locatelli, F. *et al.* (2008) Genotype-phenotype correlation in cases of juvenile myelomonocytic leukemia with clonal RAS mutations. *Blood*, **111**, 966–967.
50. Takagi, M., Piao, J., Lin, L., Kawaguchi, H., Imai, C., Ogawa, A., Watanabe, A., Akiyama, K., Kobayashi, C., Mori, M. *et al.* (2013) Autoimmunity and persistent RAS-mutated clones long after the spontaneous regression of JMML. *Leukaemia*, **27**, 1926–1928.
51. Park, H.D., Lee, S.H., Sung, K.W., Koo, H.H., Jung, N.G., Cho, B., Kim, H.K., Park, I.A., Lee, K.O., Ki, C.S. *et al.* (2012) Gene mutations in the Ras pathway and the prognostic implication in Korean patients with juvenile myelomonocytic leukemia. *Ann. Hematol.*, **91**, 511–517.
52. Sakaguchi, H., Okuno, Y., Muramatsu, H., Yoshida, K., Shiraishi, Y., Takahashi, M., Kon, A., Sanada, M., Chiba, K., Tanaka, H. *et al.* (2013) Exome sequencing identifies secondary mutations of SETBP1 and JAK3 in juvenile myelomonocytic leukemia. *Nat. Genet.*, **45**, 937–941.
53. Van der Burgt, I., Berends, E., Lommen, E., van Beersum, S., Hamel, B. and Mariman, E. (1994) Clinical and molecular studies in a large Dutch family with Noonan syndrome. *Am. J. Med. Genet.*, **53**, 187–191.
54. Allanson, J.E. (1987) Noonan syndrome. *J. Med. Genet.*, **24**, 9–13.
55. Sarkozy, A., Digilio, M.C. and Dallapiccola, B. (2008) LEOPARD syndrome. *Orphanet J. Rare Dis.*, **3**, 13.
56. Voron, D.A., Hatfield, H.H. and Kalkhoff, R.K. (1976) Multiple lentigines syndrome: case report and review of the literature. *Am. J. Med.*, **60**, 447–456.
57. Roberts, A., Allanson, J., Jadico, S.K., Kavamura, M.I., Noonan, J., Opitz, J.M., Young, T. and Neri, G. (2006) The cardiofaciocutaneous syndrome. *J. Med. Genet.*, **43**, 833–842.
58. Pérez, B., Kosmider, O., Cassinat, B., Renneville, A., Lachenaud, J., Kaltenbach, S., Bertrand, Y., Baruchel, A., Chomienne, C., Fontenay, M. *et al.* (2010) Genetic typing of CBL, ASXL1, RUNX1, TET2 and JAK2 in juvenile myelomonocytic leukaemia reveals a genetic profile distinct from chronic myelomonocytic leukaemia. *Br. J. Haematol.*, **151**, 460–468.
59. Guex, N. and Peitsch, M.C. (1997) SWISS-MODEL and the Swiss-PdbViewer: an environment for comparative protein modeling. *Electrophoresis*, **18**, 2714–2723.
60. Martinelli, S., Torreri, P., Tinti, M., Stella, L., Bocchinfuso, G., Flex, E., Grottesi, A., Ceccarini, M., Palleschi, A., Cesareni, G. *et al.* (2008) Diverse driving forces underlie the invariant occurrence of the T42A, E139D, I282V and T468M SHP2 amino acid substitutions causing Noonan and LEOPARD syndromes. *Hum. Mol. Genet.*, **17**, 2018–2029.
61. Bocchinfuso, G., Stella, L., Martinelli, S., Flex, E., Carta, C., Pantaleoni, F., Pispisa, B., Venanzi, M., Tartaglia, M. and Palleschi, A. (2007) Structural and functional effects of disease-causing amino acid substitutions affecting residues Ala72 and Glu76 of the protein tyrosine phosphatase SHP-2. *Proteins*, **66**, 963–974.
62. Darden, T., York, D. and Pedersen, L. (1993) Particle mesh Ewald: an N · log(N) method for Ewald sums in large systems. *J. Chem. Phys.*, **98**, 10089–10092.
63. Berendsen, H.J.C., Postma, J.P.M., van Gunsteren, W.F., Di Nola, A. and Haak, J.R. (1984) Molecular dynamics with coupling to an external bath. *J. Chem. Phys.*, **81**, 3684–3690.
64. Gremer, L., Merbitz-Zahradnik, T., Dvorsky, R., Cirstea, I.C., Kratz, C.P., Zenker, M., Wittinghofer, A. and Ahmadian, M.R. (2011) Germline KRAS mutations cause aberrant biochemical and physical properties leading to developmental disorders. *Hum. Mutat.*, **32**, 33–43.
65. Hemsath, L. and Ahmadian, M.R. (2005) Fluorescence approaches for monitoring interactions of Rho GTPases with nucleotides, regulators, and effectors. *Methods*, **37**, 173–182.
66. Jaiswal, M., Dubey, B.N., Koessmeier, K.T., Gremer, L. and Ahmadian, M.R. (2012) Biochemical assays to characterise Rho GTPases. *Methods Mol. Biol.*, **827**, 37–58.
67. Eberth, A. and Ahmadian, M.R. (2009) In vitro GEF and GAP assays. *Curr. Protoc. Cell Biol.*, **43**, 14.9.1–14.9.25.
68. Cirstea, I.C., Gremer, L., Dvorsky, R., Zhang, S.C., Piekorz, R.P., Zenker, M. and Ahmadian, M.R. (2013) Diverging gain-of-function mechanisms of two novel KRAS mutations associated with Noonan and cardio-facio-cutaneous syndromes. *Hum. Mol. Genet.*, **22**, 262–270.
69. Sulston, J.E. and Hodgkin, J. (1988) Methods. In Wood, W.B. and The Community of *C. elegans* Researchers (ed.), *The Nematode Caenorhabditis Elegans*. Cold Spring Harbor Laboratory Press, Cold Spring Harbor, NY, pp. 587–606.
70. Mello, C.C., Kramer, J.M., Stinchcomb, D. and Ambros, V. (1991) Efficient gene transfer in *C. elegans*: extrachromosomal maintenance and integration of transforming sequences. *EMBO J.*, **10**, 3959–3970.

Human Molecular Genetics, 2014, Vol. 23, No. 24 **6553–6566**
doi:10.1093/hmg/ddu376
Advance Access published on July 17, 2014

New *BRAF* knockin mice provide a pathogenetic mechanism of developmental defects and a therapeutic approach in cardio-facio-cutaneous syndrome

Shin-ichi Inoue[1], Mitsuji Moriya[1], Yusuke Watanabe[4], Sachiko Miyagawa-Tomita[5,6], Tetsuya Niihori[1], Daiju Oba[1], Masao Ono[2], Shigeo Kure[3], Toshihiko Ogura[4], Yoichi Matsubara[1,7] and Yoko Aoki[1,*]

[1]Department of Medical Genetics, [2]Department of Pathology, [3]Department of Pediatrics, Tohoku University School of Medicine, Sendai, Japan, [4]Department of Developmental Neurobiology, Institute of Development, Aging and Cancer, Tohoku University, Sendai, Japan, [5]Department of Pediatric Cardiology, [6]Division of Cardiovascular Development and Differentiation, Medical Research Institute, Tokyo Women's Medical University, Tokyo, Japan and [7]National Research Institute for Child Health and Development, Tokyo, Japan

Received March 15, 2014; Revised and Accepted July 14, 2014

Cardio-facio-cutaneous (CFC) syndrome is one of the 'RASopathies', a group of phenotypically overlapping syndromes caused by germline mutations that encode components of the RAS–MAPK pathway. Germline mutations in *BRAF* cause CFC syndrome, which is characterized by heart defects, distinctive facial features and ectodermal abnormalities. To define the pathogenesis and to develop a potential therapeutic approach in CFC syndrome, we here generated new knockin mice (here $Braf^{Q241R/+}$) expressing the *Braf* Q241R mutation, which corresponds to the most frequent mutation in CFC syndrome, Q257R. $Braf^{Q241R/+}$ mice manifested embryonic/neonatal lethality, showing liver necrosis, edema and craniofacial abnormalities. Histological analysis revealed multiple heart defects, including cardiomegaly, enlarged cardiac valves, ventricular noncompaction and ventricular septal defects. $Braf^{Q241R/+}$ embryos also showed massively distended jugular lymphatic sacs and subcutaneous lymphatic vessels, demonstrating lymphatic defects in RASopathy knockin mice for the first time. Prenatal treatment with a MEK inhibitor, PD0325901, rescued the embryonic lethality with amelioration of craniofacial abnormalities and edema in $Braf^{Q241R/+}$ embryos. Unexpectedly, one surviving pup was obtained after treatment with a histone 3 demethylase inhibitor, GSK-J4, or NCDM-32b. Combination treatment with PD0325901 and GSK-J4 further increased the rescue from embryonic lethality, ameliorating enlarged cardiac valves. These results suggest that our new *Braf* knockin mice recapitulate major features of RASopathies and that epigenetic modulation as well as the inhibition of the ERK pathway will be a potential therapeutic strategy for the treatment of CFC syndrome.

INTRODUCTION

Cardio-facio-cutaneous (CFC) syndrome is an autosomal dominant congenital anomaly syndrome, characterized by a distinctive facial appearance, short stature, congenital heart defects, intellectual disability and ectodermal abnormalities such as sparse, fragile hair, hyperkeratotic skin lesions and a severe generalized ichthyosis-like condition (1). The cardiac defects observed in CFC syndrome include pulmonary valve stenosis, hypertrophic cardiomyopathy and atrial septal defects. Increased nuchal translucency/fatal cystic hygroma colli due to lymphatic defects is also occasionally observed in affected individuals (2).

*To whom correspondence should be addressed at: Department of Medical Genetics, Tohoku University School of Medicine, 1-1 Seiryo-machi, Aoba-ku, Sendai 980-8574, Japan. Tel: +81 227178139; Fax: +81 227178142; Email: aokiy@med.tohoku.ac.jp

Our group as well as another group has identified germline *BRAF* mutations in 50–75% of patients with CFC syndrome (3–6). Other known CFC-causative genes include *KRAS* as well as *MAP2K1* and *MAP2K2* (MEK1 and MEK2, respectively) (3–6), all located in the same RAS–MAPK pathway that regulates cell differentiation, proliferation, survival and apoptosis (7). Germline mutations associated with RAS–MAPK pathway components cause partially overlapping disorders, including Noonan syndrome, Costello syndrome, LEOPARD syndrome, neurofibromatosis type 1 and Legius syndrome (neurofibromatosis type 1-like syndrome). These syndromes are now collectively termed RASopathies or RAS–MAPK syndromes (8–10).

BRAF is a serine threonine kinase which regulates the RAS–MAPK signaling pathway. Somatic *BRAF* mutations have been identified in 7% of human tumors, including melanoma, papillary thyroid carcinoma, colon cancer and ovarian cancer (11). The *BRAF* V600E mutation, located in the catalytic kinase domain (conserved region (CR) 3 domain), accounts for 90% of all somatic *BRAF* mutations. In contrast, *BRAF* V600E mutation has not been identified in CFC syndrome. Germline *BRAF* mutations in CR3 kinase domain, including G464R, G469E and L597V, were overlapping those in somatic mutations (4,5,12,13). In contrast, germline mutations in the CR1 domain have been rarely identified in somatic cancers. The most frequent mutations identified in CFC syndrome patients are substitutions of the residue Gln257 (p.Q257R and p.Q257K) in the CR1 domain, which account for ~40% (13). Previous studies have shown that the activation of downstream signaling, including ELK transactivation, is weaker in cells expressing the Q257R mutation than in those expressing V600E (3).

Braf is ubiquitously expressed in murine organs at mid-gestation, and high levels of its expression are found in the brain and testes at adult stage (14,15). *Braf* knockout mice have been found to die at mid-gestation from vascular defects due to enlarged blood vessels and apoptotic death of dif ferentiated endothelial cells (16). Heterozygous knockin mice constitutively expressing V600E mutation have been found to exhibit embryonic lethality (17). Knockin mice expressing a hypomorphic *BRAF* V600E allele have been reported to show phenotypes partially overlapping those of CFC syndrome patients, including small size, craniofacial abnormalities and epileptic seizures (18). However, no mouse model for CFC syndrome expressing a *Braf* mutation in the CR1 domain has been generated and no therapeutic approach has been developed. In the present study, we generated knockin mice expressing CFC syndrome-associated *Braf* Q241R mutation, corresponding to *BRAF* Q257R mutation, in order to investigate the molecular pathogenesis and potential therapeutic possibilities for CFC syndrome.

RESULTS

Generation of a CFC syndrome mouse model

We have previously reported that the transcriptional activity of ELK, downstream of ERK, was enhanced by the transient overexpression of human *BRAF* Q257R in NIH3T3 cells (3). To verify whether the expression of mouse *Braf* Q241R enhances ELK transcription as *BRAF* Q257R, reporter assays were performed in NIH3T3 cells. The expression of *Braf* Q241R and that of V637E, which corresponds to *BRAF* V600E, were ~2.7- and 8.4-fold higher than that of *Braf* WT, respectively (Fig. 1A). These results suggest that the *Braf* Q241R mutation is a gain-of-function mutation, although the activation is weaker than that observed in *Braf* V637E.

To investigate the gain-of-function effect of the *Braf* Q241R mutation on development, *Braf* Q241R knockin mice were generated (Fig. 1B). The targeting vector (Fig. 1B) was electroporated into ES cells and targeted clones were identified by Southern blotting (Fig. 1C). Appropriate ES cells were injected into BALB/c blastocysts and chimeras were obtained from six independent ES cell clones (hereafter referred to as $Braf^{Q241R\ Neo/+}$). To induce ubiquitous expression of *Braf* Q241R in germ cells, the $Braf^{Q241R\ Neo/+}$ mice were crossed with CAG-Cre transgenic mouse ($Braf^{+/+}$; *Cre*) and genotyping was confirmed by PCR (Supplementary Material, Fig. S1). Furthermore, sequencing was performed to confirm that Cre recombination resulted in *Braf* Q241R expression (Fig. 1D).

To examine if cell signaling pathways, including ERK, JNK, p38 and PI3K–AKT pathways, were altered in $Braf^{Q241R/+}$; *Cre* embryos, western blotting analysis was performed using cell extracts derived from whole-mouse embryos and brain. Protein levels of BRAF, CRAF, phosphorylated MEK and ERK in $Braf^{Q241R/+}$; *Cre* whole embryos were similar to those of $Braf^{+/+}$; *Cre* (Fig. 1E; Supplementary Material, Table S1), whereas phosphorylated MEK protein levels were higher in the brain of $Braf^{Q241R/+}$; *Cre* embryos (Fig. 1F; Supplementary Material, Table S2). Unexpectedly, phosphorylated p38 and AKT (Thr308) protein levels were somewhat lower in $Braf^{Q241R/+}$; *Cre* whole embryos at embryonic day (E) 14.5 (Fig. 1E; Supplementary Material, Table S1). These results suggest that $Braf^{Q241R/+}$; *Cre* embryos at E14.5 show a decrease of phosphorylated p38 and AKT (Thr308) protein levels.

Germline expression of *Braf* Q241R results in embryonic/neonatal lethality

Genotype analysis of embryos from an intercross between $Braf^{+/+}$; *Cre* and $Braf^{Q241R\ Neo/+}$ mice showed no surviving $Braf^{Q241R/+}$; *Cre* littermates at weaning, whereas $Braf^{+/+}$, $Braf^{+/+}$; *Cre* and $Braf^{Q241R\ Neo/+}$ littermates survived (Table 1). A normal Mendelian ratio was observed by E14.5. However, the survival rate of $Braf^{Q241R/+}$; *Cre* embryos dropped after E16.5. At E16.5, ~9.8% of embryos (4 of 41) were grossly hemorrhagic and edematous such as nuchal translucency (Fig. 2A, Table 1). Other $Braf^{Q241R/+}$; *Cre* embryos appeared normal (Fig. 2B) with no difference in body weight (data not shown). $Braf^{Q241R/+}$; *Cre* embryos, which were delivered by cesarean section at E18.5 and E19.5, remained pale and without movement or gasped for breath with cyanotic appearance, resulting in death within a few hours. A few embryos showed mandibular hypoplasia (2 of 39, 5.1%) and kyphosis (Fig. 2C and D).

Gross observation showed increased heart size in $Braf^{Q241R/+}$; *Cre* embryos at E16.5. At E18.5, $Braf^{Q241R/+}$; *Cre* embryos revealed severe peripheral liver necrosis (15 of 17, 88%) with decreased liver size and liver weight (Fig. 2E; Supplementary Material, Fig. S2). At E16.5, decreased liver weight was already observed (data not shown), although the gross appearance of the liver appeared normal. To examine if delayed lung maturation causes neonatal lethality, the histology of lung in

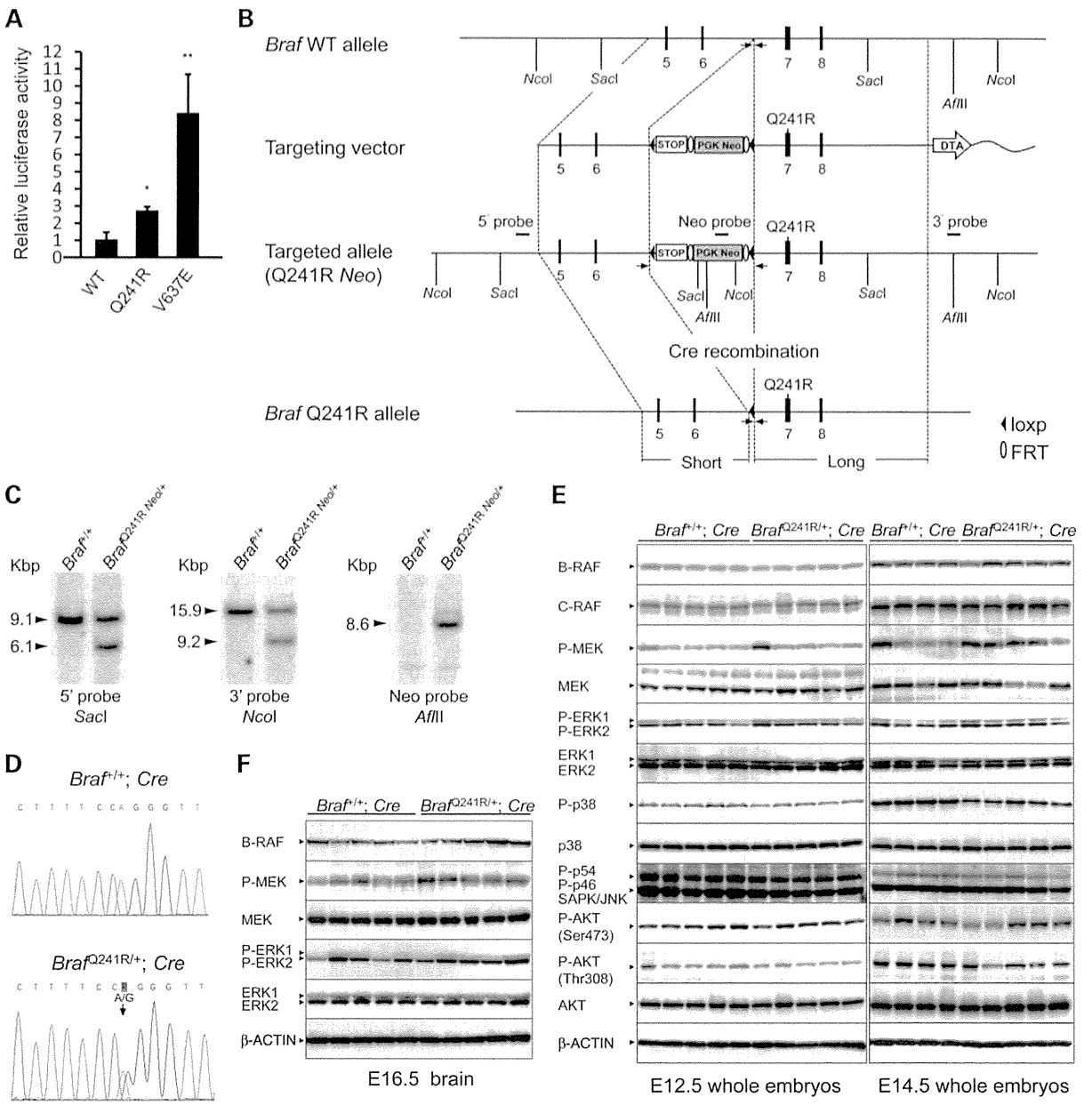

Figure 1. Generation of *Braf* Q241R knockin mice. (**A**) NIH 3T3 cells were transfected with the ELK1-GAL4 vector, the GAL4-luciferase trans-reporter vector, phRLnull-luc control vector and each mouse *Braf* expression plasmid, and reporter activities were determined as described in Materials and Methods. Luciferase activities were normalized with phRLnull-luc activities, containing distinguishable *R. reniformis* luciferase. Data are the means ± SD ($n = 4$). p.V637E in mouse *Braf* corresponds to oncogenic p.V600E in human *BRAF*. *, $P < 0.05$, **, $P < 0.01$ versus WT. WT, wild type. (**B**) Exons (solid boxes), PGK-Neomycin (PGK-Neo) cassette (gray box), STOP transcriptional sequences (open box), loxp sites (arrowheads) and Flp recombination target sites (ellipses) are indicated. Cleavage sites for diagnostic enzymes (*Sac*I, *Nco*I and *Afl*II) and the probes (5′-, 3′- and Neo probe) used to identify the homologous recombination are indicated. The PGK-Neo cassette was removed by crossing with CAG-Cre transgenic mice ($Braf^{+/+}$; *Cre*). The arrow indicates the positions of PCR primers used for genotyping of positive ES cells and mice. p. Q241R in mouse *Braf* corresponds to p.Q257R in human *BRAF*. DTA, diphtheria toxin A. (**C**) Southern blotting of ES cell clones. Genomic DNA from $Braf^{+/+}$ and $Braf^{Q241R\ Neo/+}$ ES cells was digested with *Sac*I (5′ probe), *Nco*I (3′ probe) or *Afl*II (Neo probe) and subjected to Southern blotting with a 5′, 3′ or Neo probe. The 5′, 3′ or Neo probe detects the 9.1-kb (*Braf* WT) and 6.1-kb ($Braf^{Q241R\ Neo/+}$) *Sac*I fragments, the 15.9 kb (*Braf* WT) and 9.2 kb ($Braf^{Q241R\ Neo/+}$) *Nco*I fragments or the 8.6 kb ($Braf^{Q241R\ Neo/+}$) *Afl*II fragment, respectively. (**D**) RNA was isolated from the brain of $Braf^{+/+}$; *Cre* and $Braf^{Q241R/+}$; *Cre* embryos at E18.5, and reverse transcribed into cDNA. Sanger sequencing was carried out using the cDNA. The arrow indicates the Q241R mutation in *Braf* exon 7. (**E** and **F**) Protein extracts from whole-mouse embryos (E12.5 and E14.5) and brain (E16.5) ($n = 4–5$ of each genotype) were subjected to western blotting with the indicated antibodies. β-Actin is shown as a loading control. The arrowheads indicate the bands corresponding to each protein.

Table 1. Genotyping of pups resulting from intercross between *Braf*$^{+/+}$; *Cre* and *Braf*$^{Q241R\ Neo/+}$ mice

Age	*Braf*$^{+/+}$	*Braf*$^{+/+}$; *Cre*	*Braf*$^{Q241R\ Neo/+}$	*Braf*$^{Q241R/+}$; *Cre*	*n*	*P*
E12.5	24	29	23	23	99	0.80
E13.5	5	14	6	6 (2 [1])	31	0.08
E14.5	19	22 (1)	23	11 (1 [1])	75	0.19
E16.5	57	60	55	34 (7 [4])	206	0.04
E18.5	16	23	20	0 (17 [4])	59	<0.0001
E19.5	11	16	11	0 (11 [1])	38	<0.01
Weaning (P21)	56	54	56	0	166	<0.0001
Expected	25%	25%	25%	25%		

Deviation from the expected Mendelian ratios was assessed by the χ^2 test. The number of dead embryos is shown in parentheses. The number of edematous embryos is shown in brackets. P: postnatal day.

Braf$^{Q241R/+}$; *Cre* embryos was examined at E18.5 and E19.5. Lungs of the mutant embryos appeared normal and were able to inflate, but ~11.1% of embryos (1 of 9) showed alveolar hemorrhage (Supplementary Material, Fig. S3). Thyroid transcription factor-1 (TTF-1; lung epithelial cells marker), pro-surfactant protein C and PAS staining showed similar levels in *Braf*$^{Q241R\ Neo/+}$ and *Braf*$^{Q241R/+}$; *Cre* embryos (Supplementary Material, Fig. S4), suggesting that lung development and maturation are normal. Gross observation suggests that *Braf*$^{Q241R/+}$; *Cre* embryos show embryonic/neonatal lethality, cardiomegaly, liver necrosis, edema and craniofacial abnormalities.

Braf$^{Q241R/+}$; *Cre* embryos display various heart defects

Because *Braf*$^{Q241R/+}$; *Cre* embryos showed cardiomegaly and liver necrosis, possibly due to heart failure (Fig. 2E), detailed histological analysis of the heart at different embryonic stages was conducted. At E12.5, the hearts of *Braf*$^{Q241R/+}$; *Cre* embryos appeared normal (Supplementary Material, Fig. S5A), but showed an enlarged pulmonary valve and a dramatic increase in the density of trabeculae (hypertrabeculation) at E14.5 (Supplementary Material, Fig. S5B). At E16.5, 13 of 14 (93%) *Braf*$^{Q241R/+}$; *Cre* embryos (excluding edematous embryos) had various heart defects (Supplementary Material, Tables S3 and S4). Hypertrophy of pulmonary, tricuspid and mitral valves was present in 7, 8 and 9 of 14 embryos, respectively (Fig. 3A; Supplementary Material, Tables S3 and S4). In particular, hypertrophy in pulmonary valve leaflets was prominent, plugging the entire space of the pulmonary valve ring (Fig. 3B). Other heart defects observed in *Braf*$^{Q241R/+}$; *Cre* embryos included ventricular septal defect (VSD) in 2 of 14 embryos (Fig. 3A), abnormal endocardial cushion in 2 (Fig. 3A), hypertrabeculation in 3 (Fig. 3A), epicardial blisters in 2 (Fig. 3A and C), a thickened trabecular layer and thinned compact layer in the left, right or combined myocardium (noncompaction: one case of cardiomyopathy accompanied by cardiac hypertrophy) in 4 (Fig. 3D) and hypoplasia of the coronary arteries in 3. The ventricular radius and the thickness of the pulmonary and tricuspid valves were significantly higher in *Braf*$^{Q241R/+}$; *Cre* embryos, suggesting cardiac enlargement and thickened pulmonary and tricuspid valves (Fig. 3E). These results suggest that *Braf*$^{Q241R/+}$; *Cre* embryos develop various congenital heart defects, which almost certainly contributes to embryonic lethality.

Braf$^{Q241R/+}$; *Cre* embryo hearts exhibit enhancement of cell proliferation, ERK signaling activation and decrease of phosphorylated p38 and AKT

To examine if heart defects observed in *Braf*$^{Q241R/+}$; *Cre* embryos are caused by increased cell proliferation and/or reduced cell death, cell proliferation was analyzed by phosphohistone H3 (pHH3) immunostaining and cell death by TUNEL assay. At E13.5, regarding heart abnormalities in each embryos, the number of pHH3-positive-stained cells varied. pHH3-positive-stained cells in the interventricular septum and myocardium increased in *Braf*$^{Q241R/+}$; *Cre* embryos (Fig. 4A and B). At E16.5, the nucleus of pHH3-positive cells increased in the interventricular septum in embryos with VSD (Fig. 4C). *Braf*$^{Q241R/+}$; *Cre* embryos had more pHH3-positive cells in pulmonary valves (Fig. 4D). In contrast to cell proliferation, hardly any cells undergoing apoptosis were observed in either *Braf*$^{+/+}$; *Cre* or *Braf*$^{Q241R/+}$; *Cre* at E13.5 and E16.5 (data not shown). These results suggest that the cell proliferation state depends on heart abnormalities in each embryo at E16.5 and that the increased staining for pHH3 in the interventricular septum was associated with VSD.

To examine if the cardiac signaling pathways were altered in *Braf*$^{Q241R/+}$; *Cre* embryos, the activation of kinases was screened in various signaling pathways using a phospho-kinase array followed by western blotting of the lysates from hearts of *Braf*$^{Q241R/+}$; *Cre* embryos at E16.5 (Fig. 4E and F; Supplementary Material, Fig. S6). No changes in phosphorylated ERK protein levels in both the phospho-kinase array and western blotting were observed. In contrast, phosphorylated p38, AKT (Ser473) and AKT (Thr308) protein levels, which are not direct targets of BRAF, were relatively lower in *Braf*$^{Q241R/+}$; *Cre* embryos than in *Braf*$^{+/+}$; *Cre*, which was confirmed by western blotting. To verify the activation of transcription factors downstream of ERK, the expression of ELK1 and the PEA3 (polyoma enhancer activator 3) subfamily Ets transcription factors were examined by quantitative real-time PCR, these expressions being known as transcriptional targets of FGF signaling-mediated activation of ERK in heart and oncogenic BRAF signaling in melanoma (19,20). At E13.5, E16.5 and E18.5, cardiac mRNA levels of *Etv1*, *Etv4* and *Etv5*, but not *Elk1*, were significantly higher in *Braf*$^{Q241R/+}$; *Cre* embryos than those in *Braf*$^{+/+}$; *Cre* (Fig. 4G; Supplementary Material, Fig. S7). Next, we investigated the influence of genes responsible for hypertrophic cardiomyopathy and

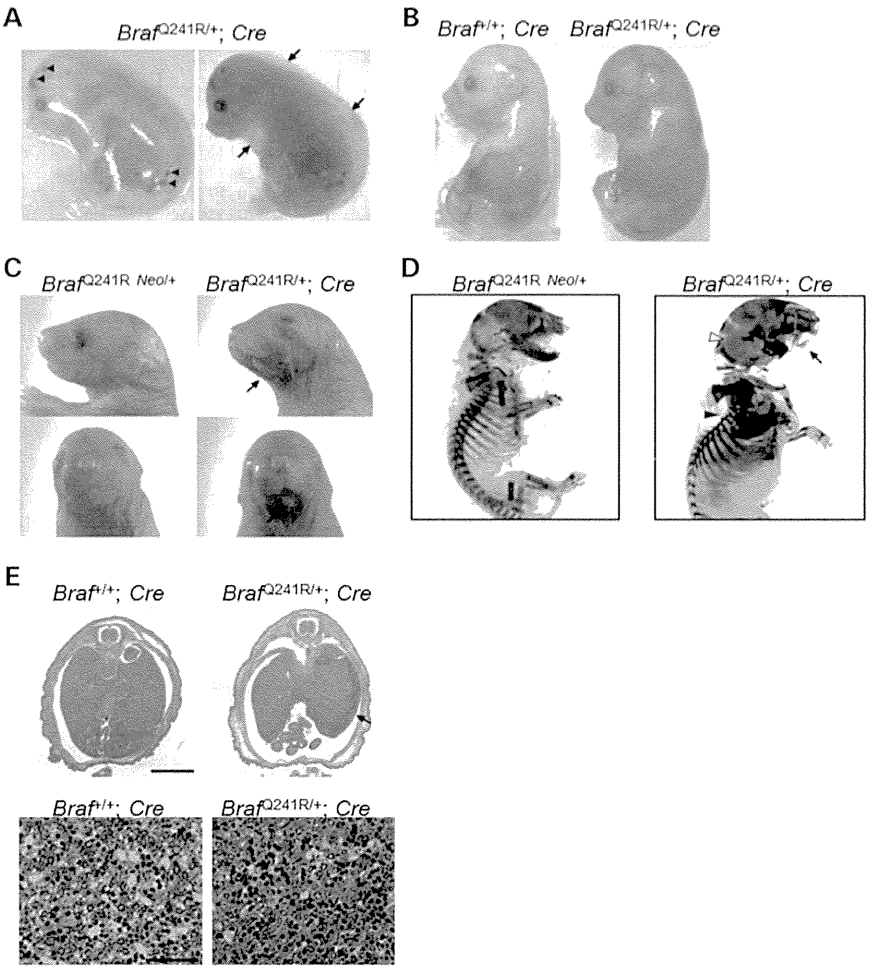

Figure 2. Lethal phenotypes of *Braf*$^{Q241R/+}$; *Cre* embryos. (**A** and **B**) Gross appearance of *Braf*$^{+/+}$; *Cre* and *Braf*$^{Q241R/+}$; *Cre* embryos at E16.5. (A) Arrowheads and arrows indicate hemorrhage and edema, respectively. The right panel shows *Braf*$^{Q241R/+}$; *Cre* embryos with transmitted illumination. (**C**) Craniofacial structure of *Braf*$^{Q241R\ Neo/+}$ and *Braf*$^{Q241R/+}$; *Cre* embryos at E19.5. The arrow indicates mandibular hypoplasia. (**D**) Alcian Blue/Alizarin Red staining of *Braf*$^{Q241R\ Neo/+}$ and *Braf*$^{Q241R/+}$; *Cre* embryos at E19.5. The arrow, solid arrowhead and open arrowhead indicate mandibular hypoplasia, kyphosis and ossification in the interparietal bone, respectively. (**E**) H&E staining of liver sections of *Braf*$^{+/+}$; *Cre* and *Braf*$^{Q241R/+}$; *Cre* embryos at E18.5. The arrow indicates hepatic necrosis. The lower panel shows higher magnification views of hepatic necrosis. Scale bars in upper panels = 200 μm and in lower panels = 50 μm.

cardiac development in *Braf*$^{Q241R/+}$; *Cre* embryos at E18.5, which exhibited a cardiomyopathy phenotype, such as cardiac enlargement and noncompaction (Fig. 3D and E) and structural abnormalities, including VSD. No differences in mRNA levels of cardiomyopathy-specific genes (*Myh6* and *Myh7)* and genes related to the heart formation and development (*Gata4* and *Nkx2.5*) were observed (Fig. 4G). These results suggest that ERK activation, including increased mRNA levels of Ets transcription factors, and decreased levels of p38 and AKT exist in heart tissues of *Braf*$^{Q241R/+}$; *Cre* embryos.

Braf$^{Q241R/+}$; *Cre* embryos develop lymphangiectasia

Patients with RASopathies, including CFC syndrome and Noonan syndrome, exhibit nuchal translucency, which is subcutaneous fluid collection in the fetal neck visualized by ultrasonography. Nuchal translucency is caused by distended jugular lymphatic sacs (JLSs), which result from a disturbance in differentiation of lymphatic endothelial cells (21,22). We hypothesized that the hemorrhage and edema in *Braf*$^{Q241R/+}$; *Cre* embryos may be caused by defective lymphatic development. Histological examination revealed distended and blood-filled JLSs in *Braf*$^{Q241R/+}$; *Cre* embryos but not in *Braf*$^{+/+}$; *Cre* embryos at E12.5 and E16.5 (Fig. 5A and B; Supplementary Material, Fig. S8A). The primary lymphatic sacs are remodeled to produce a hierarchically organized network of lymphatic capillaries and collecting lymph vessels at stages between E14.5 and postnatal stages (23). The JLSs are hardly observed in mouse embryos at E16.5. In *Braf*$^{Q241R/+}$; *Cre* embryos at E16.5, cavities such as the JLSs of mouse embryos from E12.5 to E14.5 were observed (Fig. 5B), suggesting defective lymphatic development from the cardinal vein in *Braf*$^{Q241R/+}$; *Cre*

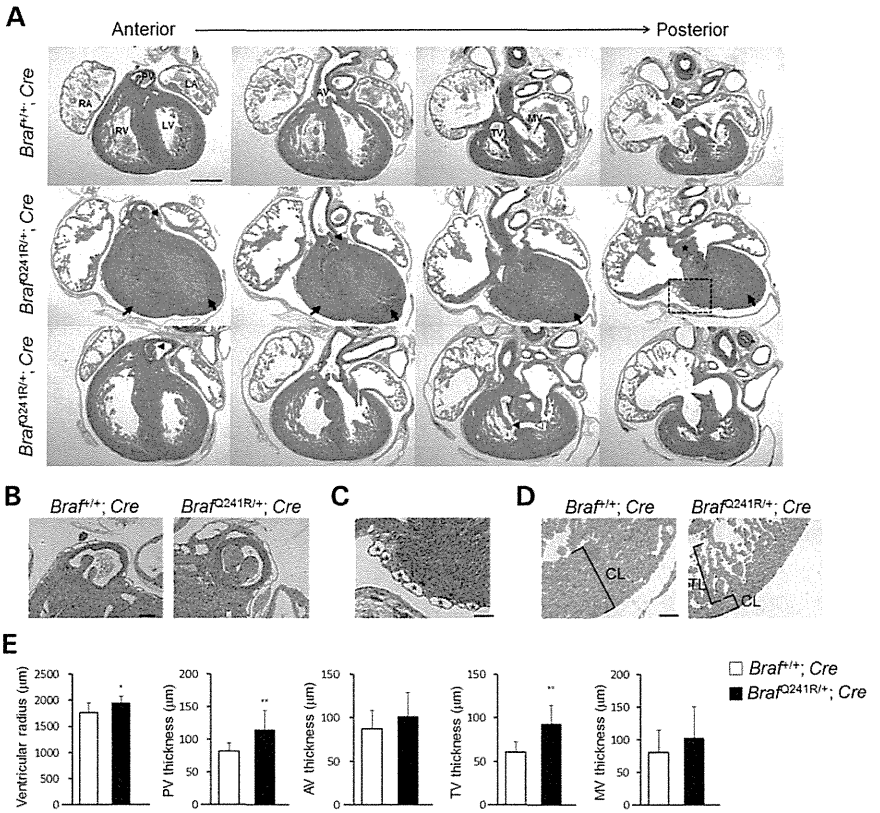

Figure 3. Cardiac phenotype of *Braf*$^{Q241R/+}$; *Cre* embryos. (**A**–**D**) H&E staining of sequential anterior to posterior sections of embryonic hearts from *Braf*$^{+/+}$; *Cre* and *Braf*$^{Q241R/+}$; *Cre* at E16.5. A dramatic increase in density of trabeculae (arrows), enlarged valves (solid arrowheads), VSD (open arrowhead) and abnormal endocardial cushion (asterisk) are observed. Scale bars 500 μm (A) and 100 μm (B–D). (B) Higher magnification of the pulmonary valves in *Braf*$^{+/+}$; *Cre* and *Braf*$^{Q241R/+}$; *Cre* embryos. (C) Higher magnification of the boxed region in Figure 3A showing the epicardial blisters (asterisks) in *Braf*$^{Q241R/+}$; *Cre* embryos at E16.5. (D) Representative image of noncompaction in hearts from *Braf*$^{Q241R/+}$; *Cre* embryos at E16.5. (**E**) The ventricular radius and the thicknesses of the cardiac valve leaflets were measured at their largest diameter in serial sections of *Braf*$^{+/+}$; *Cre* and *Braf*$^{Q241R/+}$; *Cre* embryos at E16.5. Data are the means ± SD (*Braf*$^{+/+}$; *Cre* ($n = 9$) and *Braf*$^{Q241R/+}$; *Cre* ($n = 14$)). $^{*}P < 0.05$, $^{**}P < 0.01$ versus *Braf*$^{+/+}$; *Cre*. LV, left ventricle; RV, right ventricle; LA, left atrium; RA, right atrium; PV, pulmonary valve; AV, aortic valve; TV, tricuspid valve; MV, mitral valve; CL, compact layer; TL, trabecular layer.

embryos. To examine the network formation of blood and lymphatic vessels, we performed immunostaining using antibodies against lymphatic vessel endothelial hyaluronan receptor 1 (LYVE-1; lymphatic endothelial cell-specific marker), α-SMA for staining of vessels with smooth muscle and CD31 (platelet-endothelial cell adhesion molecule-1, PECAM-1) for staining of vascular endothelial cells. At E12.5, the cells lining JLSs in both *Braf*$^{+/+}$; *Cre* and *Braf*$^{Q241R/+}$; *Cre* embryos were positive for LYVE-1 (Fig. 5C), whereas slightly CD31-positive cells were detected in JLSs and the jugular vein (Fig. 5D). No α-SMA expression was observed (Supplementary Material, Fig. S8B). At E16.5, the cavities such as the JLSs in *Braf*$^{Q241R/+}$; *Cre* embryos were negative for LYVE-1, α-SMA and CD31 (Fig. 5E; Supplementary Material, Fig. S8C and D), but the subcutaneous lymphatic vessels were markedly positive for LYVE-1 (Fig. 5F; Supplementary Material, Fig. S8E). These results indicate that *Braf*$^{Q241R/+}$; *Cre* embryos show defective lymphatic development from the cardinal vein, leading to distention of the JLSs, dilated lymphatic vessels and edema.

Treatment with a MEK inhibitor and/or histone demethylase inhibitors prevents embryonic lethality in *Braf*$^{Q241R/+}$; *Cre* embryos

MEK inhibitor, PD0325901, treatment is known to rescue the embryonic lethality of Noonan syndrome model mice (24). Pregnant *Braf*$^{+/+}$; *Cre* mice were treated with various compounds to see whether this would result in recovery from embryonic lethality (Table 2). Male *Braf*$^{Q241R\ Neo/+}$ mice were crossed with female *Braf*$^{+/+}$; *Cre* mice, and pregnant mice were intraperitoneally injected with dimethylsulfoxide (vehicle), PD0325901 [0.5 or 1.0 mg of body weight (mg/kg)], MAZ51 (VEGFR3 inhibitor; 1.0, 2.0 or 5.0 mg/kg), sorafenib (BRAF, VEGFR, PDGFR multikinase inhibitor; 5.0 mg/kg), lovasatin (HMG-CoA reductase and farnesyl transferase inhibitor; 5.0 mg/kg) or everolimus (mTOR inhibitor; 0.1 mg/kg), daily from E10.5 to E18.5. PD0325901 treatment (0.5 mg/kg) modestly rescued the embryonic lethality of *Braf*$^{Q241R/+}$; *Cre* mice (2 of 30). Seven embryos also survived for 3 weeks with

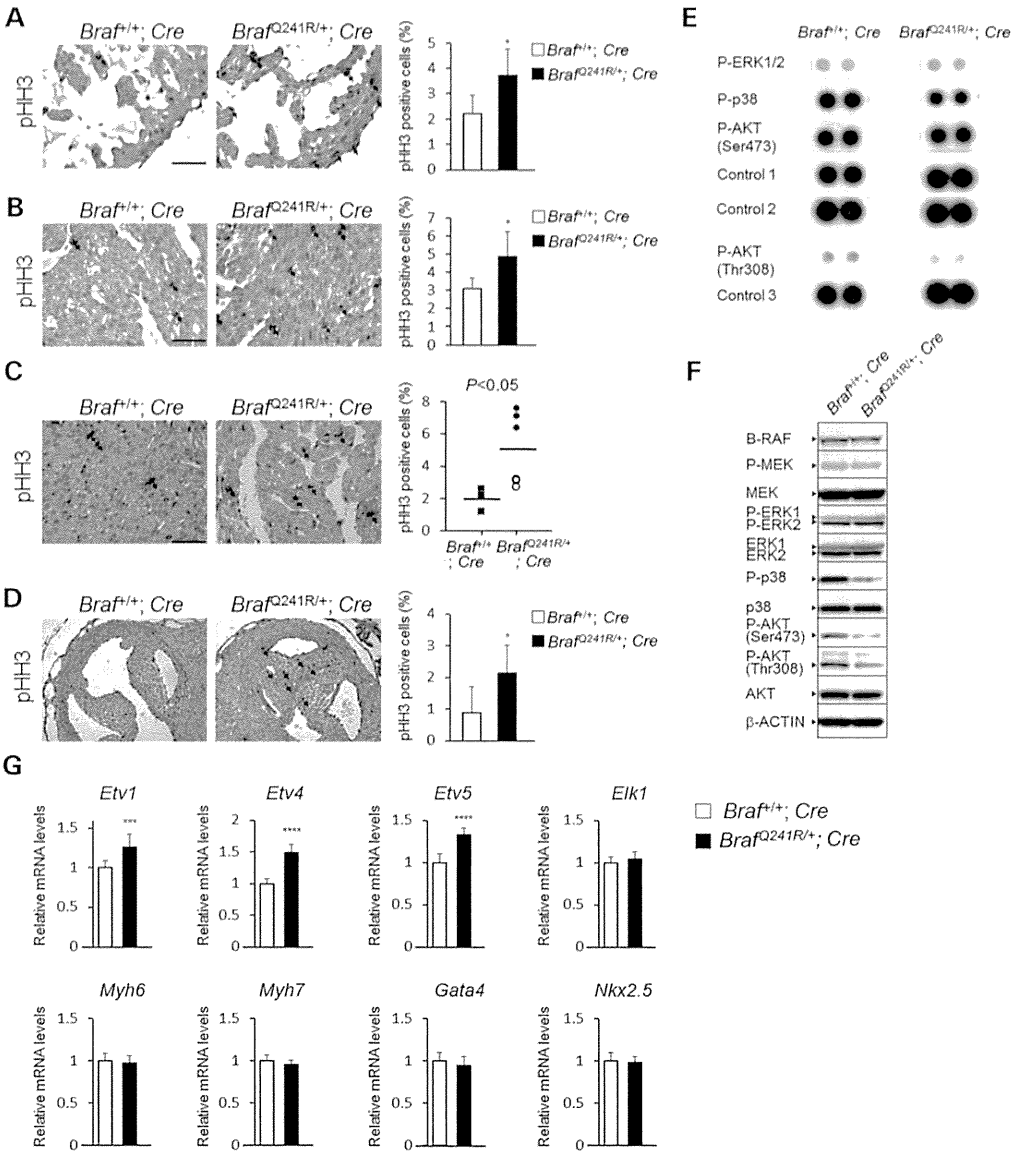

Figure 4. Increased cell proliferation and altered multiple signaling pathways in *Braf*$^{Q241R/+}$; *Cre* embryo hearts. (**A**–**D**) Immunostaining for pHH3 in the myocardium (A), interventricular septum (B and C) and pulmonary valves (D) of *Braf*$^{+/+}$; *Cre* and *Braf*$^{Q241R/+}$; *Cre* embryos at E13.5 (A and B) and E16.5 (C and D). The arrows indicate representative positive cells. *Braf*$^{Q241R/+}$; *Cre* embryos with or without VSD are shown in closed cycles or open circles, respectively. Scale bars 50 μm (A–C). Data are means ± SD (A and B) *Braf*$^{+/+}$; *Cre* ($n = 5$) and *Braf*$^{Q241R/+}$; *Cre* ($n = 5$). (C and D) *Braf*$^{+/+}$; *Cre* ($n = 3$) and *Braf*$^{Q241R/+}$; *Cre* ($n = 6$). $^{*}P < 0.05$ versus *Braf*$^{+/+}$; *Cre*. (**E**) Protein extracts (400 μg) of the hearts from *Braf*$^{+/+}$; *Cre* and *Braf*$^{Q241R/+}$; *Cre* embryos at E16.5 were subjected to Phospho-Kinase Antibody Array. Results are representative of gene spots that showed significant changes in 45 phosphorylated proteins. (**F**) Western blotting of the hearts from *Braf*$^{+/+}$; *Cre* and *Braf*$^{Q241R/+}$; *Cre* embryos at E16.5 (pooled samples; *Braf*$^{+/+}$; *Cre* ($n = 5$), *Braf*$^{Q241R/+}$; *Cre* ($n = 5$)). β-Actin is shown as a loading control. The arrowheads indicate the bands corresponding to each protein. (**G**) Cardiac mRNA levels were determined by quantitative reverse transcription–PCR. mRNA levels were normalized by those of *Gapdh*, and those in *Braf*$^{+/+}$; *Cre* at E18.5 are set at 1. Data are the means ± SD (*Braf*$^{+/+}$; *Cre* ($n = 10$) and *Braf*$^{Q241R/+}$; *Cre* ($n = 6$)). $^{***}P < 0.001$, $^{****}P < 0.0001$ versus *Braf*$^{+/+}$; *Cre*. *Etv1*, *Etv4*, *Etv5*, *Myh6* and *Myh7* encode ER81, Pea3, ERM, α-MHC and β-MHC, respectively.

prenatal treatment of PD0325901 (1.0 mg/kg) (7 of 37, $P = 0.32$, χ^2 test for deviation from the Mendelian ratios). PD0325901-treated *Braf*$^{Q241R/+}$; *Cre* embryos appeared normal without edema and mandibular hypoplasia (0 of 31 at E16.5 to P0), whereas other genotype mice, excluding *Braf*$^{Q241R/+}$; *Cre* treated with PD0325901, showed teratogenic effects, including open eyes (Supplementary Material, Fig. S9), edema, enlarged semilunar valves and atrioventricular valves (data not shown). Other compounds had no effect on the recovery of embryonic lethality in *Braf*$^{Q241R/+}$; *Cre* embryos.

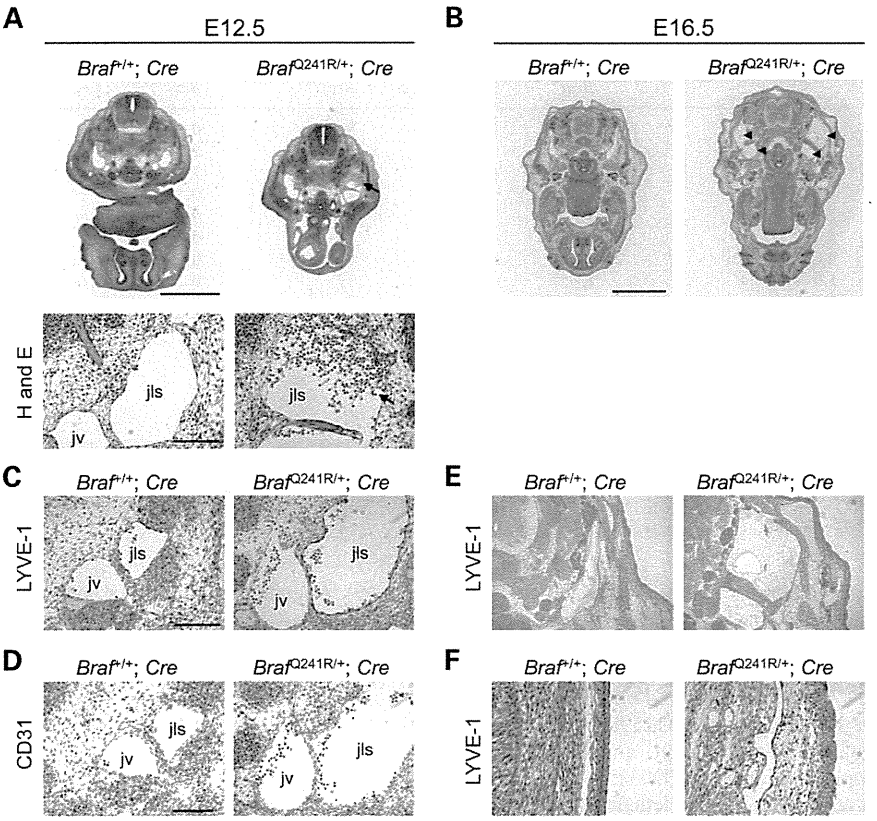

Figure 5. Abnormal lymphatic development in *Braf*$^{Q241R/+}$; *Cre* embryos. (**A** and **B**) Transverse sections of *Braf*$^{+/+}$; *Cre* and *Braf*$^{Q241R/+}$; *Cre* embryos at E12.5 (A) and E16.5 (B) stained with H&E. Lower panels show high-magnification views of jugular lymph sac (A). The arrows (A) and arrowheads (B) indicate blood cells in jugular lymph sacs and the regions which are similar to the jugular lymph sacs or jugular veins of embryos at E12.5, respectively. Scale bars 1 mm (in upper panels, A), 100 μm (in lower panels, A) and 2 mm (B). (**C**–**F**) Sections of *Braf*$^{+/+}$; *Cre* and *Braf*$^{Q241R/+}$; *Cre* embryos at E12.5 (C and D) and E16.5 (E and F) stained with antibodies against lymphatic endothelial markers, LYVE-1 (C, E and F) or CD31 (D). (F) Subcutaneous lymphatic vessels. jls, jugular lymph sac; jv, jugular vein.

Thus, PD0325901 treatment prevented embryonic lethality in *Braf*$^{Q241R/+}$; *Cre* embryos and could ameliorate edema and mandibular hypoplasia.

Epigenetic regulation of gene expression, such as histone acetylation and histone methylation, plays a crucial role in the transcriptional regulation of cell differentiation, development, the inflammatory response and cancer (25). Recently, a histone deacetylase inhibitor, SAHA [vorinostat (Zolinza)], has been used in the treatment of lymphomas and solid tumors. Recent studies have suggested the association of UTX and JMJD3, a histone H3 lysine 27 (H3K27) demethylase, with heart development (26–28). We therefore tested whether treatment using these compounds leads to the rescue of embryonic lethality (Table 2). SAHA treatment had no effect (data not shown); however, one embryo survived for 3 weeks with prenatal treatment of GSK-J4 (inhibitors of histone H3K27 demethylase UTX and JMJD3; 5.0 mg/kg) (25) or NCDM-32b (inhibitor of histone H3K9 demethylase JMJD2C; 5.0 mg/kg) (29). Moreover, co-treatment with GSK-J4 (5.0 mg/kg) and PD0325901 (0.5 mg/kg) further increased the number of *Braf*$^{Q241R/+}$; *Cre* mice alive at weaning (5 of 31, $P = 0.14$). The teratogenic effects, which were frequently observed in PD0325901 treatment, were not observed in the co-treatment with GSK-J4 and PD0325901.

We further investigated whether co-treatment with PD0325901 and GSK-J4 prevented heart defects in *Braf*$^{Q241R/+}$; *Cre* embryos. Co-treatment with PD0325901 and GSK-J4, but not PD0325901 treatment (1.0 mg/kg) alone, ameliorated enlarged pulmonary, tricuspid and mitral valves in *Braf*$^{Q241R/+}$; *Cre* embryos (Fig. 6A and B). However, no difference in the frequency of heart defects, including VSD, hypertrabeculation, epicardial blisters and non-compaction, was observed. It is noteworthy that treatment with PD0325901 or GSK-J4 alone or the co-treatment reversed the decrease of phosphorylated p38 protein levels (Fig. 6C; Supplementary Material, Fig. S10). These results suggest that combination treatment with PD0325901 and GSK-J4 prevents embryonic lethality, enlarged cardiac valves and decreased phosphorylated p38 in *Braf*$^{Q241R/+}$; *Cre* embryos.

DISCUSSION

In this study, we generated heterozygous *Braf* Q241R-expressing mice, which exhibited embryonic and postnatal lethality due to liver necrosis, skeletal abnormalities, lymphatic defects and various cardiac defects, including cardiomegaly, non-compaction, enlarged cardiac valves and hypertrabeculation.

Table 2. Rescue of embryonic lethality in *Braf*$^{Q241R/+}$; *Cre* embryos by MEK inhibitor, histone demethylase inhibitor or these combined treatment

Compound	Dose (mg/kg body weight)	Genotype (3 weeks)				n^a	n^b	n^c	P
		Braf$^{+/+}$	*Braf*$^{+/+}$; *Cre*	*Braf*$^{Q241R\ Neo/+}$	*Braf*$^{Q241R/+}$; *Cre*				
DMSO (vehicle)	–	14	8	8	0	30	6	5.0	<0.01
PD0325901	0.5	7	14	7	2	30	13	2.3	0.02
	1.0	11	13	6	7	37	14	2.6	0.32
MAZ51	1.0	9	8	11	0	28	6	4.7	0.02
	2.0	10	14	7	0	31	6	5.2	<0.01
	5.0	10	7	11	0	28	11	2.5	0.01
Sorafenib	5.0	12	15	8	0	35	13	2.7	<0.01
Lovastatin	5.0	8	19	17	0	44	10	4.4	<0.01
Everolimus	0.1	6	6	9	0	21	9	2.3	0.04
NCDM-32b	2.0	12	4	9	0	25	9	2.8	<0.01
	5.0	10	10	14	1	35	11	3.2	0.02
	10.0	11	10	19	0	40	9	4.4	<0.01
GSK-J4	5.0	8	18	14	1	41	11	3.7	<0.01
	10.0	16	26	20	0	62	23	2.7	<0.01
PD0325901 + GSK-J4	0.5 + 5.0	8	13	5	5	31	10	3.1	0.14

Male *Braf*$^{Q241R\ Neo/+}$ mice were crossed with female *Braf*$^{+/+}$; *Cre* mice, and pregnant mice were intraperitoneally injected with vehicle or various compounds shown daily from E10.5 to E18.5. Deviation from the expected Mendelian ratios was assessed by χ^2 test. n^a, the total number of acquired pups. n^b, the total number of treated female *Braf*$^{+/+}$; *Cre* mice. n^c, the average number of survived pups at weaning (n^a/n^b).

Increased expression of Ets transcription factors and decreased expression of cardiac phosphorylated p38 in embryonic heart tissues were observed. PD0325901 treatment, in part, rescued embryonic and postnatal lethality in *Braf*$^{Q241R/+}$; *Cre* mice. One pup in *Braf*$^{Q241R/+}$; *Cre* also survived until P21 with treatment of GSK-J4 or NCDM-32b. PD0325901 treatment, but not GSK-J4 and NCDM-32b treatment, ameliorated edema and mandibular hypoplasia. Moreover, PD0325901 co-treatment with GSK-J4 further rescued embryonic lethality with recovered hypertrophy of pulmonary, tricuspid and mitral valves and the decreased expression of phosphorylated p38. Taken together, mice expressing a development-specific *Braf* Q241R mutation will be useful to further clarify the pathogenesis of CFC syndrome and to develop therapeutic approaches.

Patients with RASopathies are characterized by generalized abnormalities of lymphatic development. Fetuses with RASopathies have been shown to be characterized by hydrops, pleural effusions, increased nuchal translucency due to distended JLS and cystic hygroma in utero (30–32). Children and adults with RASopathies show generalized lymphedema, peripheral lymphoedema or pulmonary lymphangiectasia (33). Our new model, *Braf*$^{Q241R/+}$; *Cre* mice, showed embryonic and postnatal lethality and exhibited multiple developmental defects in the lymphatic system, including hydrops, distended JLS and subcutaneous lymphatic vessels. In contrast, mice of other knockin mouse models for RASopathies survived to adulthood and have not shown the defects in lymphatic system (34–36). Thus, for the first time our new model *Braf*$^{Q241R/+}$; *Cre* mice demonstrated the developmental lymphatic defects, which are the common features observed in RASopathies, in knockin mouse models for RASopathies.

Dysregulation of the RAS–MAPK pathway is a common underlying mechanism of RASopathies. However, a variety of compounds, including the RAS–MAPK pathway and other signaling pathways, has been effective for ameliorating the defects in previous knockin mouse models of RASopathies. MEK inhibitors have been found to ameliorate the cardiac defects and skeletal features in mice expressing *SOS1* and *RAF1* mutations (24,35). Angiotensin II inhibitor ameliorates the phenotypes of hypertension, vascular remodeling and fibrosis of the kidney and heart in mice expressing *HRAS* G12V mutation (36), and mTOR inhibitor ameliorates hypertrophic cardiomyopathy in a mouse model of LEOPARD syndrome, expressing a catalytically inactive mutation in SHP2 (34). We examined a variety of compounds, including anti-cancer agents, MEK inhibitor, mTOR inhibitor, VEGFR3 inhibitor, BRAF inhibitor and farnesyl transferase inhibitor using our *Braf*$^{Q241R/+}$; *Cre* mice. Treatment with MEK inhibitor, but not mTOR inhibitor, in *Braf*$^{Q241R/+}$; *Cre* mice ameliorated embryonic lethality and skeletal abnormalities, suggesting that the pathogenesis of the disease is similar to those in *SOS1* and *RAF1* mutations. Thus, our new *Braf*$^{Q241R/+}$; *Cre* mice will be useful to screen various compounds for therapeutic approaches to RASopathies.

The exact mechanisms by which the single treatment of histone demethylase inhibitor or co-treatment of MEK inhibitor and histone demethylase inhibitor were effective for *Braf*$^{Q241R/+}$; *Cre* mice have not yet been characterized. Lysine modification of histone 3, acetylation and methylation, is associated with gene activation or silencing (37). In gene expression, inactive genes show methylation at lysine 27, and permanently silenced genes frequently are characterized by methylation at lysine 9 (37). Histone H3K27 methylase, *Ezh2*, conditional knockout mice in cardiomyocytes have been reported to show abnormal heart development, such as noncompaction and excessive trabeculation (38). Meanwhile, deletion of histone H3K27 demethylase, UTX, has been identified in individuals with Kabuki syndrome, who showed distinctive facial appearance and congenital heart disease (39). H3K9 methyltransferases, G9a and GLP, have been shown to be essential for cardiac morphogenesis (40). It is of note that the balance between methylation and demethylation of H3 is required for normal cardiac differentiation. *De novo* mutations in *SMAD2*, a transcription factor which regulates H3K27 methylation in embryonic left–right organizer, have been identified in children with congenital heart disease (28). *SMAD2*, which is regulated by ERK (41), has been found to bind to H3K27 demethylase JMJD3, and regulate H3K27 methylation

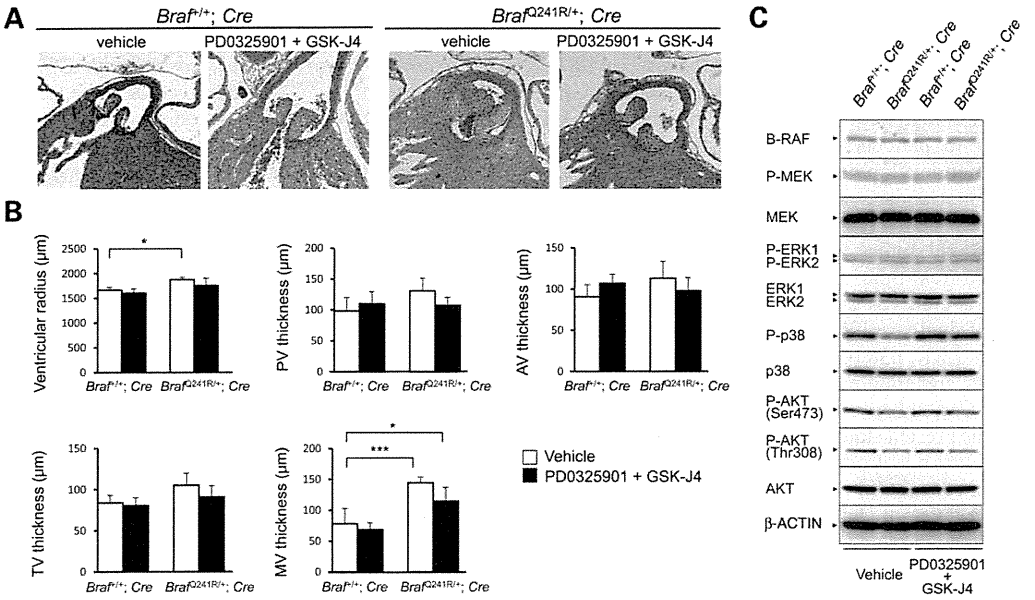

Figure 6. Influence of co-treatment with PD0325901 and GSK-J4 on the cardiac phenotype and signaling of *Braf*$^{Q241R/+}$; *Cre* embryos. (**A** and **B**) Sequential sections of embryonic hearts from *Braf*$^{+/+}$; *Cre* and *Braf*$^{Q241R/+}$; *Cre* at E16.5 stained H&E. (A) Histological sections of pulmonary valves. (B) The ventricular radius and the thicknesses of the cardiac valve leaflets were measured at their largest diameter in serial sections. Data are means ± SD (vehicle; *Braf*$^{+/+}$; *Cre* ($n = 5$), *Braf*$^{Q241R/+}$; *Cre* ($n = 5$). PD0325901 + GSK-J4; *Braf*$^{+/+}$; *Cre* ($n = 7$), *Braf*$^{Q241R/+}$; *Cre* ($n = 11$)). $^{*}P < 0.05$, $^{***}P < 0.001$ (Tukey–Kramer test). NS, not significant. (**C**) Western blotting of the hearts from *Braf*$^{+/+}$; *Cre* and *Braf*$^{Q241R/+}$; *Cre* embryos at E16.5 (vehicle-treated pooled samples; *Braf*$^{+/+}$; *Cre* ($n = 8$), *Braf*$^{Q241R/+}$; *Cre* ($n = 8$). PD0325901 + GSK-J4-treated pooled samples; *Braf*$^{+/+}$; *Cre* ($n = 8$), *Braf*$^{Q241R/+}$; *Cre* ($n = 7$)). β-Actin is shown as a loading control. The arrowheads indicate the bands corresponding to each protein.

(28), suggesting that the histone demethylase JMJD3 is associated with heart development in humans by indirect regulation of ERK. In addition, constitutively activated BRAF and RAS mutants, through ERK activation, have been shown to induce JMJD3 and EZH2 expression (42,43). These observations suggest that activation of BRAF or ERK is associated with histone H3K27 modification, regulating cardiac development. In this study, the total content of the H3K27me3 in heart tissues of *Braf*$^{Q241R/+}$; *Cre* or *Braf*$^{Q241R/+}$; *Cre* mice after GSK-J4 co-treatment with PD0325901 was comparable with that of *Braf*$^{+/+}$; *Cre* mice (data not shown). Furthermore, the histone H3K27 demethylase activity of lysates from *Braf*$^{Q241R/+}$; *Cre* embryos at E14.5 was comparable with that of *Braf*$^{+/+}$; *Cre* (data not shown). Further analysis of H3K9 and H3K27 modification status on individual genes will clarify the mechanism by which histone demethylase inhibitor is effective against embryonic and postnatal lethality and developmental defects in *Braf*$^{Q241R/+}$; *Cre* mice.

MEK inhibitor treatment or crossing with ERK1 knockout mice has improved the hypertrophy of cardiac valves in Noonan syndrome model mice with a *SOS1* or *PTPN11* mutation (24,44). In contrast, treatment of MEK inhibitor did not lead to the amelioration of enlarged cardiac valves in *Braf*$^{Q241R/+}$; *Cre* embryos. Furthermore, other mice, excluding *Braf*$^{Q241R/+}$; *Cre*, treated with MEK inhibitor showed enlarged cardiac valves (data not shown), suggesting that the vital nature of MEK/ERK signaling balance in cardiac valve development. Given that no MEK inhibitor activity nor the inhibition activity of other protein kinases has been reported in GSK-J1 (GSK-J4 sodium salt) (25), these results suggest that not only MEK/ERK signaling balance but also histone H3K27 modification can play a crucial role in the normal development of cardiac valve in *Braf*$^{Q241R/+}$; *Cre* embryos.

The natural history and the frequency of tumors in adult CFC patients have not been fully elucidated (6). Since molecular analysis became available, three individuals with *BRAF* mutation have been reported to have developed acute lymphoblastic leukemia and non-Hodgkin lymphoma (6). Knockin mice expressing *BRAF* L597V mutation survived to adulthood and showed multiple Noonan syndrome/CFC syndrome phenotypes, including short stature, facial dysmorphia and cardiac enlargement (12). The L597V is located in the CR3 kinase domain and leads to 2-fold elevated BRAF kinase activity (45). The L597V mutation has been identified in 11 somatic cancers (COSMIC; http://cancer.sanger.ac.uk/cancergenome/projects/cosmic/) and three patients with Noonan syndrome (13,46,47), which generally shows milder phenotype than that in CFC syndrome. In contrast, Q257R mutation is located in the CR1 domain and has been identified in 40% of CFC syndrome, not in cancers. Our ELK transactivation study has shown that level of ELK transactivation in Q257R was a half of V600E (3). The previous report showed that BRAF Q257R has increased BRAF kinase activity compared with WT and the activity was as high as that of the V600E (4). It is possible that differences in kinase activity and/or the effect on downstream pathways could cause the phenotypic differences in these knockin mice. Surviving *Braf*$^{Q241R/+}$; *Cre* mice in the PD0325901 treatment showed distinctive facial appearance, abnormal dental occlusion, reduced postnatal length and weight, kyphosis and skin

disease, which are similar to CFC syndrome phenotype (data not shown) (1,48). *Braf*$^{Q241R/+}$; *Cre* mice also survived to adulthood when these mice (C57BL/6J background) were crossed with ICR or BALB/c mice (unpublished data). Further studies will be necessary to examine if adult *Braf*$^{Q241R/+}$; *Cre* mice show phenotypes similar to patients with CFC syndrome, including seizures and tumor development.

The potential mechanism of activation and downregulation of multiple signaling pathways in *Braf*$^{Q241R/+}$; *Cre* embryos is unclear. In additional studies, we performed microarray analysis and quantitative real-time PCR using heart tissues from *Braf*$^{Q241R/+}$; *Cre* embryos at E13.5 or E16.5. Interestingly, mRNA levels of dual specificity phosphatase (*Dusp*) 2, 4 and 6, that inactivate ERK, p38 or JNK, and *Spry* 1, which inhibits the RAS–MAPK signaling pathway, were significantly higher in *Braf*$^{Q241R/+}$; *Cre* embryos than those in *Braf*$^{+/+}$; *Cre* (data not shown). In the present study, constitutive activation of phosphorylated ERK was not clearly observed in whole embryos and heart tissues from *Braf*$^{Q241R/+}$; *Cre*. These results suggest that increased mRNA levels of *Dusp* 2, 4, 6 and *Spry* 1 and decreased expression of phosphorylated p38 in embryonic heart could represent a negative feedback mechanism for normalizing constitutive ERK activation in *Braf*$^{Q241R/+}$; *Cre* embryos.

In summary, *Braf* Q241R-expressing mice provided an effective tool for studying the pathogenesis of CFC syndrome. It was found for the first time that combination treatment with PD0325901 and GSK-J4 is efficacious for the treatment of mice with the activation of the RAS–MAPK pathway. At present, clinical trials of a new MEK inhibitor, MEK162, are now being conducted to investigate the efficacy and safety of its use in Noonan syndrome with hypertrophic cardiomyopathy as well as in individuals with solid tumors, while no clinical trial of histone H3K27 demethylase inhibitor has been performed. Given that *BRAF* mutations cause cancer, combination therapy with MEK inhibitors and histone H3K27 demethylase inhibitors can be effective not only for the treatment of patients with RASopathies but also for the treatment of *BRAF* mutation-associated cancer in the future.

MATERIALS AND METHODS

Generation of *Braf*^{Q241R} knockin mice

To construct the targeting vector for *Braf*^{Q241R} knockin mice, a short arm containing *Braf* exon 5 and 6 (*Not*I-*Sac*II genomic DNA fragment), a long arm including exon 7, 8 (*Xma*I–*Bam*HI genomic DNA fragment) and the downstream of exon 8 (*Bam*HI–*Sac*I) were amplified using a Roswell Park Cancer Institute-23 BAC clone. The DNA fragments were ligated into the pBSIISK+ vector. The *Braf* Q241R (exon 7) mutation was introduced by site-directed mutagenesis. The *Psp*0MI–*Xho*I site was used to insert PGK-Neo-STOP cassette flanked by loxP sites. The targeting vector was linearized with *Sal*I and electroporated into ES cells (C57BL/6J background). To confirm correctly targeted ES clones, we performed genotyping, sequencing and the test of the Cre-mediated recombination system. Furthermore, homologous recombinants were confirmed by Southern blotting using 5′, 3′ and Neo probes. For this experiment, genomic DNA was digested with *Sac*I (5′ probe), *Nco*I (3′ probe) or *Afl*II (Neo probe). The probe sequences are shown in Supplementary Material, Table S5. Screened ES clones were then microinjected into BALB/c blastocytes and the resulting chimeras were crossed with C57BL/6J mice to obtain *Braf*$^{Q241R\ Neo/+}$ heterozygotes mice. Excisions of the PGK-Neo cassette and STOP codon were achieved by crossing of *Braf*$^{Q241R\ Neo/+}$ heterozygotes with CAG-Cre transgenic mice (*Braf*$^{+/+}$; *Cre*) on C57BL/6J background (RIKEN BioResource Center, Tsukuba, Japan; RBRC01828) (49). Animal experiments were approved by the Animal Care and Use Committee of Tohoku University.

Genotyping

Genomic DNA was prepared from tail tissue with DNeasy Blood & Tissue Kit (Qiagen, Hilden, Germany) or Maxwell 16 Mouse Tail DNA Purification Kit (Promega, Madison, WI, USA). Genotyping of the *Braf*$^{+/+}$, *Braf*$^{+/+}$; *Cre*, *Braf*$^{Q241R\ Neo/+}$ and *Braf*$^{Q241R/+}$; *Cre* was carried out by PCR using KOD FX Neo (TOYOBO, Osaka, Japan) or TaKaRa Taq (Takara Bio, Otsu, Japan) with the primers shown in Supplementary Material, Table S6.

Sequencing

Total RNA was extracted with TRIzol reagent (Invitrogen, Carlsland, CA, USA), and cDNA was synthesized using High-Capacity cDNA Reverse Transcription Kit (Applied Biosystems, Foster City, CA, USA). The exonic region in *Braf* was amplified by PCR using TaKaRa Taq with the primers including M13 sequences: 5′-GTAAAACGACGGCCAGTGAAGTACT GGAGAATGTCCC-3′ and 5′-AGGAAACAGCTATGACCC CACATGTTTGACAACGGAAACCC-3′. The PCR products were purified with QIAquick Gel Extraction Kit (Qiagen, Tokyo, Japan) and sequenced on an ABI 3500xl automated DNA sequencer (Applied Biosystems).

Quantitative reverse transcription–PCR

Quantitative PCR was performed using FastStart Universal Probe Master (ROX) (Applied Biosystems) with StepOnePlus (Applied Biosystems). Amplification primers and hydrolysis probes were designed using Universal ProbeLibrary Assay Design Center (https://qpcr.probefinder.com/roche3.html).

Alcian Blue/Alizarin Red staining

After embryos were placed in water for a day, the skin and viscera were removed. The eviscerated embryos were then fixed in 95% ethanol for at least 3 days and stained with 150 mg/l Alcian Blue 8GX (Sigma-Aldrich, St Louis, MO, USA), 80% ethanol and 20% acetic acid for 16–24 h. The stained embryos were rinsed with 95% ethanol and kept in 2% KOH for 16–24 h. They were then stained with 50 mg/l Alizarin Red (Sigma-Aldrich) and 1% KOH for 3 h, kept in 2% KOH for 12–48 h, placed in 20% glycerin/1% KOH for at least 5 days and stored in 50% glycerin.

Plasmid construction

The expression construct, including mouse *Braf* cDNA, was purchased from Origene (Rockville, MD, USA). PCR was performed using primers designed to introduce *Hin*dIII sites and the V5 epitope (C terminus). The PCR fragment was subcloned into pCR4-TOPO Vector (Invitrogen). The entire cDNA was verified by sequencing. The mutant constructs for *Braf* Q241R and V637E were generated using QuikChange Lightning Site-Directed Mutagenesis Kit (Stratagene, La Jolla, CA, USA) with the primers, 5′-CCGAAAGCTGCTTTTCCGGGGTTT CCGTTGTCAAA-3′ and 5′-TTTGACAACGGAAACCCCGG AAAAGCAGCTTTCGG-3′, and 5′-CTTTGGTCTAGCCACA GAGAAATCTCGGTGGAGTG-3′ and 5′-CACTCCACCGA GATTTCTCTGTGGCTAGACCAAAG-3′, respectively. All mutant constructs were verified by sequencing. The cDNAs were digested with *Hin*dIII, blunt-ended with T4 DNA polymerase and ligated into blunt-ended *Eco*RI site of pCAGGS vector (50).

Reporter assay

NIH 3T3 cells (ATCC, Rockville, MD, USA) were maintained in Dulbecco's modified Eagle's medium supplemented with 10% newborn calf serum, 50 U/ml penicillin and 50 μg/ml of streptomycin. The cells were seeded in 24-well plates at 3×10^5 cells/well 24 h before transfection. The cells were then transiently transfected using Lipofectamine and PLUS Reagent (Invitrogen) with 400 ng of pFR-luc, 25 ng of pFA2-Elk1, 5 ng of phRLnull-luc and 5 ng of WT or mutant expression constructs of *Braf*. Forty-eight hours after transfection, the cells were harvested in passive lysis buffer, and luciferase activity was assayed using Dual-Luciferase Reporter Assay System (Promega). Renilla luciferase expressed by phRLnull-luc was used to normalize the transfection efficiency.

Western blotting and phospho-kinase-antibody array

Whole-mouse embryos and brain were lysed in lysis buffer (10 mM Tris–HCl, pH 8.0 and 1% SDS), or genotype-confirmed hearts were pooled and lysed in the same buffer. These lysates were centrifuged at 14 000*g* for 15 min at 4°C and the protein concentration was determined by the Bradford method with Bio-Rad Protein Assay (Bio-Rad Laboratories, Hercules, CA, USA). Lysates were subjected to SDS–polyacrylamide gel electrophoresis (5–20% gradient gel; ATTO, Tokyo, Japan) and transferred to nitrocellulose membrane. Antibodies used were as follows (with catalog numbers in parentheses): B-RAF (9434), ERK1/2 (9102), phospho-ERK1/2 (9101), phospho-MEK (9121), p38 (9212), phospho-p38 (4511), phospho-SAPK/JNK (4668), AKT (9272), phospho-AKT (on Ser473; 9018) and phospho-AKT (on Thr308; 2965) from Cell Signaling (Danvers, MA, USA). C-RAF (610152), MEK (sc-219) and β-actin (A5316) were from BD Transduction Laboratories (San Jose, CA, USA), Santa Cruz Biotechnology (Santa Cruz, CA, USA) and Sigma-Aldrich, respectively. All the membranes were visualized using Western Lightning ECL-Plus Kit (Perkin-Elmer, Waltham, MA, USA). The band intensities were quantified using ImageJ software (http://rsbweb.nih.gov/ij/) and normalized to β-actin. Phosphorylated protein was measured to determine the ratios of phosphorylated protein to non-phosphorylated protein and then normalized to β-actin.

For kinase-antibody arrays, protein extracts of embryonic hearts (400 μg) were incubated with the Phospho-Kinase Antibody Array Kit (Proteome Profiler Antibody Array; R&D systems, Minneapolis, MN, USA) following the manufacturer's instructions.

Histology and immunohistochemistry

Embryonic hearts were perfused with phosphate-buffered saline and 10% neutral buffered formalin from the placenta. The fixed hearts and whole-mouse embryos fixed in 10% neutral buffered formalin were embedded in paraffin. Embedded tissues were sectioned at 6 μm (hearts) or 3 μm (whole-mouse embryos and lungs). Sections were stained with hematoxylin and eosin. In hearts from embryos at E16.5, the largest diameters of the ventricular radius were measured in serial coronal sections where a four-chamber view was observed. The largest thicknesses of cardiac valve leaflets in serial sections were measured. Edematous and dead embryos were excluded from these analyses.

For immunohistochemistry, the antibodies used were as follows (with catalog numbers in parentheses): phospho-Histone H3 (9701) from Cell Signaling, LYVE-1 (103-PA50AG) from RELIA Tech GmbH (Braunschweig, Germany), α-SMA (M0851) from DAKO (Glostrup, Denmark), PECAM-1 (CD31; sc-1506) from Santa Cruz Biotechnology and TTF-1 (MS-669-P1ABX) from Thermo Fisher Scientific (Fremont, CA, USA). Signals were amplified by Histofine Simple Stain (Nichirei Bio Sciences, Tokyo, Japan) and color was developed by DAB Substrate Kit (Nichirei Bio Sciences). Sections were counterstained with hematoxylin.

PAS staining

Deparaffinized lung sections were incubated in 0.5% periodic acid for 10 min at 60°C, rinsed with distilled water and stained in Schiff's reagent (Muto Pure Chemicals, Tokyo, Japan) for 10 min. Stained slides were counterstained with hematoxylin, dehydrated and mounted.

Animal treatment

Stock solution of PD0325901 (Sigma-Aldrich) was prepared using ethanol, whereas those of MAZ-51 (Calbiochem, San Diego, CA, USA), Sorafenib (Toronto Research Chemicals, North York, ON, USA), Lovastatin (Calbiochem), Everolimus (Selleckchem, Houston, TX, USA), NCDM-32b (Wako Pure Chemicals, Osaka, Japan), GSK-J4 (Cayman Chemical) and the combination of PD0325901 and GSK-J4 were prepared using dimethylsulfoxide. PD0325901 was resuspended in saline while and all other reagents were resuspended in 0.5% hydroxypropylmethylcellulose with 0.2% Tween80, respectively. The prepared reagents or vehicles were i.p. injected into pregnant mice daily, beginning on E10.5 and continuing till E15.5 or E18.5.

Statistical analysis

All statistical analysis was performed using Prism software (ver. 6.01; GraphPad Software, Inc., San Diego, CA, USA). Data analysis were performed with Student's *t*-test for unpaired samples, one-way analysis of variance followed by the Tukey–Kramer test for comparison of multiple experimental groups and the χ^2 test for differences between observed and expected distributions. Differences were considered significant at a *P*-value of < 0.05.

SUPPLEMENTARY MATERIAL

Supplementary Material is available at *HMG* online.

ACKNOWLEDGEMENTS

We are grateful to Jun-ichi Miyazaki, Osaka University, for supplying the pCAGGS expression vector. We thank Riyo Takahashi, Kumi Kato, Yoko Tateda and Daisuke Akita for technical assistance and Fumiko Date for technical assistance and for discussion of the experimental data. We also acknowledge the support of the Biomedical Research Core of Tohoku University Graduate School of Medicine. We thank RIKEN BioResource Center for providing us with B6.Cg-Tg(CAG-Cre)CZ-MO2Osb mice (RBRC01828).

Conflict of Interest statement. None declared.

FUNDING

This work was supported by the Funding Program for the Next Generation of World-Leading Researchers (NEXT Program) from the Ministry of Education, Culture, Sports, Science and Technology of Japan to Y.A. (LS004), by Grants-in-Aids from the Ministry of Education, Culture, Sports, Science and Technology of Japan, the Ministry of Health, Labor and Welfare, and the Japan Society for the Promotion of Science (JSPS) KAKENHI Grant number 26293241 to Y.A., and by JSPS KAKENHI Grant number 25860839 to S.I.

REFERENCES

1. Reynolds, J.F., Neri, G., Herrmann, J.P., Blumberg, B., Coldwell, J.G., Miles, P.V. and Opitz, J.M. (1986) New multiple congenital anomalies/mental retardation syndrome with cardio-facio-cutaneous involvement – the CFC syndrome. *Am. J. Med. Genet.*, **25**, 413–427.
2. Witters, I., Denayer, E., Brems, H., Fryns, J.P. and Legius, E. (2008) The cardiofaciocutaneous syndrome: prenatal findings in two patients. *Prenat. Diagn.*, **28**, 53–55.
3. Niihori, T., Aoki, Y., Narumi, Y., Neri, G., Cave, H., Verloes, A., Okamoto, N., Hennekam, R.C., Gillessen-Kaesbach, G., Wieczorek, D. *et al.* (2006) Germline KRAS and BRAF mutations in cardio-facio-cutaneous syndrome. *Nat. Genet.*, **38**, 294–296.
4. Rodriguez-Viciana, P., Tetsu, O., Tidyman, W.E., Estep, A.L., Conger, B.A., Cruz, M.S., McCormick, F. and Rauen, K.A. (2006) Germline mutations in genes within the MAPK pathway cause cardio-facio-cutaneous syndrome. *Science*, **311**, 1287–1290.
5. Narumi, Y., Aoki, Y., Niihori, T., Neri, G., Cave, H., Verloes, A., Nava, C., Kavamura, M.I., Okamoto, N., Kurosawa, K. *et al.* (2007) Molecular and clinical characterization of cardio-facio-cutaneous (CFC) syndrome: overlapping clinical manifestations with Costello syndrome. *Am. J. Med. Genet. A*, **143A**, 799–807.
6. Abe, Y., Aoki, Y., Kuriyama, S., Kawame, H., Okamoto, N., Kurosawa, K., Ohashi, H., Mizuno, S., Ogata, T., Kure, S. *et al.* (2012) Prevalence and clinical features of Costello syndrome and cardio-facio-cutaneous syndrome in Japan: findings from a nationwide epidemiological survey. *Am. J. Med. Genet. A*, **158A**, 1083–1094.
7. Malumbres, M. and Barbacid, M. (2003) RAS oncogenes: the first 30 years. *Nat. Rev. Cancer*, **3**, 459–465.
8. Aoki, Y., Niihori, T., Banjo, T., Okamoto, N., Mizuno, S., Kurosawa, K., Ogata, T., Takada, F., Yano, M., Ando, T. *et al.* (2013) Gain-of-function mutations in RIT1 cause Noonan syndrome, a RAS/MAPK pathway syndrome. *Am. J. Hum. Genet.*, **93**, 173–180.
9. Aoki, Y., Niihori, T., Narumi, Y., Kure, S. and Matsubara, Y. (2008) The RAS/MAPK syndromes: novel roles of the RAS pathway in human genetic disorders. *Hum. Mutat.*, **29**, 992–1006.
10. Tidyman, W.E. and Rauen, K.A. (2009) The RASopathies: developmental syndromes of Ras/MAPK pathway dysregulation. *Curr. Opin. Genet. Dev.*, **19**, 230–236.
11. Davies, H., Bignell, G.R., Cox, C., Stephens, P., Edkins, S., Clegg, S., Teague, J., Woffendin, H., Garnett, M.J., Bottomley, W. *et al.* (2002) Mutations of the BRAF gene in human cancer. *Nature*, **417**, 949–954.
12. Andreadi, C., Cheung, L.K., Giblett, S., Patel, B., Jin, H., Mercer, K., Kamata, T., Lee, P., Williams, A., McMahon, M. *et al.* (2012) The intermediate-activity (L597 V) BRAF mutant acts as an epistatic modifier of oncogenic RAS by enhancing signaling through the RAF/MEK/ERK pathway. *Genes Dev.*, **26**, 1945–1958.
13. Sarkozy, A., Carta, C., Moretti, S., Zampino, G., Digilio, M.C., Pantaleoni, F., Scioletti, A.P., Esposito, G., Cordeddu, V., Lepri, F. *et al.* (2009) Germline BRAF mutations in Noonan, LEOPARD, and cardiofaciocutaneous syndromes: molecular diversity and associated phenotypic spectrum. *Hum. Mutat.*, **30**, 695–702.
14. Storm, S.M., Cleveland, J.L. and Rapp, U.R. (1990) Expression of raf family proto-oncogenes in normal mouse tissues. *Oncogene*, **5**, 345–351.
15. Wojnowski, L., Stancato, L.F., Larner, A.C., Rapp, U.R. and Zimmer, A. (2000) Overlapping and specific functions of Braf and Craf-1 proto-oncogenes during mouse embryogenesis. *Mech. Dev.*, **91**, 97–104.
16. Wojnowski, L., Zimmer, A.M., Beck, T.W., Hahn, H., Bernal, R., Rapp, U.R. and Zimmer, A. (1997) Endothelial apoptosis in Braf-deficient mice. *Nat. Genet.*, **16**, 293–297.
17. Mercer, K., Giblett, S., Green, S., Lloyd, D., DaRocha Dias, S., Plumb, M., Marais, R. and Pritchard, C. (2005) Expression of endogenous oncogenic V600E B-raf induces proliferation and developmental defects in mice and transformation of primary fibroblasts. *Cancer Res.*, **65**, 11493–11500.
18. Urosevic, J., Sauzeau, V., Soto-Montenegro, M.L., Reig, S., Desco, M., Wright, E.M., Canamero, M., Mulero, F., Ortega, S., Bustelo, X.R. *et al.* (2011) Constitutive activation of B-Raf in the mouse germ line provides a model for human cardio-facio-cutaneous syndrome. *Proc. Natl. Acad. Sci. USA*, **108**, 5015–5020.
19. Watanabe, Y., Miyagawa-Tomita, S., Vincent, S.D., Kelly, R.G., Moon, A.M. and Buckingham, M.E. (2010) Role of mesodermal FGF8 and FGF10 overlaps in the development of the arterial pole of the heart and pharyngeal arch arteries. *Circ. Res.*, **106**, 495–503.
20. Packer, L.M., East, P., Reis-Filho, J.S. and Marais, R. (2009) Identification of direct transcriptional targets of (V600E)BRAF/MEK signalling in melanoma. *Pigment Cell Melanoma Res.*, **22**, 785–798.
21. Deng, Y., Atri, D., Eichmann, A. and Simons, M. (2013) Endothelial ERK signaling controls lymphatic fate specification. *J. Clin. Invest.*, **123**, 1202–1215.
22. Bekker, M.N., Twisk, J.W., Bartelings, M.M., Gittenberger-de Groot, A.C. and van Vugt, J.M. (2006) Temporal relationship between increased nuchal translucency and enlarged jugular lymphatic sac. *Obstet. Gynecol.*, **108**, 846–853.
23. Makinen, T., Norrmen, C. and Petrova, T.V. (2007) Molecular mechanisms of lymphatic vascular development. *Cell Mol. Life Sci.*, **64**, 1915–1929.
24. Chen, P.C., Wakimoto, H., Conner, D., Araki, T., Yuan, T., Roberts, A., Seidman, C., Bronson, R., Neel, B., Seidman, J.G. *et al.* (2010) Activation of multiple signaling pathways causes developmental defects in mice with a Noonan syndrome-associated Sos1 mutation. *J. Clin. Invest.*, **120**, 4353–4365.
25. Kruidenier, L., Chung, C.W., Cheng, Z., Liddle, J., Che, K., Joberty, G., Bantscheff, M., Bountra, C., Bridges, A., Diallo, H. *et al.* (2012) A selective jumonji H3K27 demethylase inhibitor modulates the proinflammatory macrophage response. *Nature*, **488**, 404–408.

26. Lee, S., Lee, J.W. and Lee, S.K. (2012) UTX, a histone H3-lysine 27 demethylase, acts as a critical switch to activate the cardiac developmental program. *Dev. Cell*, **22**, 25–37.
27. Welstead, G.G., Creyghton, M.P., Bilodeau, S., Cheng, A.W., Markoulaki, S., Young, R.A. and Jaenisch, R. (2012) X-linked H3K27me3 demethylase Utx is required for embryonic development in a sex-specific manner. *Proc. Natl. Acad. Sci. USA*, **109**, 13004–13009.
28. Zaidi, S., Choi, M., Wakimoto, H., Ma, L., Jiang, J., Overton, J.D., Romano-Adesman, A., Bjornson, R.D., Breitbart, R.E., Brown, K.K. *et al.* (2013) De novo mutations in histone-modifying genes in congenital heart disease. *Nature*, **498**, 220–223.
29. Hamada, S., Suzuki, T., Mino, K., Koseki, K., Oehme, F., Flamme, I., Ozasa, H., Itoh, Y., Ogasawara, D., Komaarashi, H. *et al.* (2010) Design, synthesis, enzyme-inhibitory activity, and effect on human cancer cells of a novel series of jumonji domain-containing protein 2 histone demethylase inhibitors. *J. Med. Chem.*, **53**, 5629–5638.
30. Croonen, E.A., Nillesen, W.M., Stuurman, K.E., Oudesluijs, G., van de Laar, I.M., Martens, L., Ockeloen, C., Mathijssen, I.B., Schepens, M., Ruiterkamp-Versteeg, M. *et al.* (2013) Prenatal diagnostic testing of the Noonan syndrome genes in fetuses with abnormal ultrasound findings. *Eur. J. Hum. Genet.*, **21**, 936–942.
31. Nisbet, D.L., Griffin, D.R. and Chitty, L.S. (1999) Prenatal features of Noonan syndrome. *Prenat. Diagn.*, **19**, 642–647.
32. de Mooij, Y.M., van den Akker, N.M., Bekker, M.N., Bartelings, M.M., van Vugt, J.M. and Gittenberger-de Groot, A.C. (2011) Aberrant lymphatic development in euploid fetuses with increased nuchal translucency including Noonan syndrome. *Prenat. Diagn.*, **31**, 159–166.
33. Romano, A.A., Allanson, J.E., Dahlgren, J., Gelb, B.D., Hall, B., Pierpont, M.E., Roberts, A.E., Robinson, W., Takemoto, C.M. and Noonan, J.A. (2010) Noonan syndrome: clinical features, diagnosis, and management guidelines. *Pediatrics*, **126**, 746–759.
34. Marin, T.M., Keith, K., Davies, B., Conner, D.A., Guha, P., Kalaitzidis, D., Wu, X., Lauriol, J., Wang, B., Bauer, M. *et al.* (2011) Rapamycin reverses hypertrophic cardiomyopathy in a mouse model of LEOPARD syndrome-associated PTPN11 mutation. *J. Clin. Invest.*, **121**, 1026–1043.
35. Wu, X., Simpson, J., Hong, J.H., Kim, K.H., Thavarajah, N.K., Backx, P.H., Neel, B.G. and Araki, T. (2011) MEK-ERK pathway modulation ameliorates disease phenotypes in a mouse model of Noonan syndrome associated with the Raf1(L613 V) mutation. *J. Clin. Invest.*, **121**, 1009–1025.
36. Schuhmacher, A.J., Guerra, C., Sauzeau, V., Canamero, M., Bustelo, X.R. and Barbacid, M. (2008) A mouse model for Costello syndrome reveals an Ang II-mediated hypertensive condition. *J. Clin. Invest.*, **118**, 2169–2179.
37. Kooistra, S.M. and Helin, K. (2012) Molecular mechanisms and potential functions of histone demethylases. *Nat. Rev. Mol. Cell. Biol.*, **13**, 297–311.
38. He, A., Ma, Q., Cao, J., von Gise, A., Zhou, P., Xie, H., Zhang, B., Hsing, M., Christodoulou, D.C., Cahan, P. *et al.* (2012) Polycomb repressive complex 2 regulates normal development of the mouse heart. *Circ. Res.*, **110**, 406–415.
39. Lederer, D., Grisart, B., Digilio, M.C., Benoit, V., Crespin, M., Ghariani, S.C., Maystadt, I., Dallapiccola, B. and Verellen-Dumoulin, C. (2012) Deletion of KDM6A, a histone demethylase interacting with MLL2, in three patients with Kabuki syndrome. *Am. J. Hum. Genet.*, **90**, 119–124.
40. Inagawa, M., Nakajima, K., Makino, T., Ogawa, S., Kojima, M., Ito, S., Ikenishi, A., Hayashi, T., Schwartz, R.J., Nakamura, K. *et al.* (2013) Histone H3 lysine 9 methyltransferases, G9a and GLP are essential for cardiac morphogenesis. *Mech. Dev.*, **130**, 519–531.
41. Kretzschmar, M., Doody, J., Timokhina, I. and Massague, J. (1999) A mechanism of repression of TGFbeta/ Smad signaling by oncogenic Ras. *Genes Dev.*, **13**, 804–816.
42. Agger, K., Cloos, P.A., Rudkjaer, L., Williams, K., Andersen, G., Christensen, J. and Helin, K. (2009) The H3K27me3 demethylase JMJD3 contributes to the activation of the INK4A-ARF locus in response to oncogene- and stress-induced senescence. *Genes Dev.*, **23**, 1171–1176.
43. Fujii, S., Tokita, K., Wada, N., Ito, K., Yamauchi, C., Ito, Y. and Ochiai, A. (2011) MEK-ERK pathway regulates EZH2 overexpression in association with aggressive breast cancer subtypes. *Oncogene*, **30**, 4118–4128.
44. Krenz, M., Gulick, J., Osinska, H.E., Colbert, M.C., Molkentin, J.D. and Robbins, J. (2008) Role of ERK1/2 signaling in congenital valve malformations in Noonan syndrome. *Proc. Natl. Acad. Sci. USA*, **105**, 18930–18935.
45. Wan, P.T., Garnett, M.J., Roe, S.M., Lee, S., Niculescu-Duvaz, D., Good, V.M., Jones, C.M., Marshall, C.J., Springer, C.J., Barford, D. *et al.* (2004) Mechanism of activation of the RAF-ERK signaling pathway by oncogenic mutations of B-RAF. *Cell*, **116**, 855–867.
46. Pierpont, E.I., Pierpont, M.E., Mendelsohn, N.J., Roberts, A.E., Tworog-Dube, E., Rauen, K.A. and Seidenberg, M.S. (2010) Effects of germline mutations in the Ras/MAPK signaling pathway on adaptive behavior: cardiofaciocutaneous syndrome and Noonan syndrome. *Am. J. Med. Genet. A*, **152A**, 591–600.
47. Stevenson, D.A., Schwarz, E.L., Carey, J.C., Viskochil, D.H., Hanson, H., Bauer, S., Weng, H.Y., Greene, T., Reinker, K., Swensen, J. *et al.* (2011) Bone resorption in syndromes of the Ras/MAPK pathway. *Clin. Genet.*, **80**, 566–573.
48. Armour, C.M. and Allanson, J.E. (2008) Further delineation of cardio-facio-cutaneous syndrome: clinical features of 38 individuals with proven mutations. *J. Med. Genet.*, **45**, 249–254.
49. Matsumura, H., Hasuwa, H., Inoue, N., Ikawa, M. and Okabe, M. (2004) Lineage-specific cell disruption in living mice by Cre-mediated expression of diphtheria toxin A chain. *Biochem. Biophys. Res. Commun.*, **321**, 275–279.
50. Niwa, H., Yamamura, K. and Miyazaki, J. (1991) Efficient selection for high-expression transfectants with a novel eukaryotic vector. *Gene*, **108**, 193–199.

Supplementary Material:

Including Supplementary Figures 1-10 and Supplementary Tables 1-6.

New *BRAF* knock-in mice provide a pathogenetic mechanism of developmental defects and a therapeutic approach in cardio-facio-cutaneous syndrome

Shin-ichi Inoue,[1] Mitsuji Moriya,[1] Yusuke Watanabe,[2] Sachiko Miyagawa-Tomita,[3,4] Tetsuya Niihori,[1] Daiju Oba,[1] Masao Ono,[5] Shigeo Kure,[6] Toshihiko Ogura,[2] Yoichi Matsubara,[1,7] and Yoko Aoki[1]

[1]Department of Medical Genetics, Tohoku University School of Medicine, Sendai, Japan.
[2]Department of Developmental Neurobiology, Institute of Development, Aging and Cancer, Tohoku University, Sendai, Japan.
[3]Department of Pediatric Cardiology, Tokyo Women's Medical University, Tokyo, Japan.
[4]Division of Cardiovascular Development and Differentiation, Medical Research Institute, Tokyo Women's Medical University, Tokyo, Japan.
[5]Department of Pathology, Tohoku University School of Medicine, Sendai, Japan.
[6]Department of Pediatrics, Tohoku University School of Medicine, Sendai, Japan.
[7]National Research Institute for Child Health and Development, Tokyo, Japan.

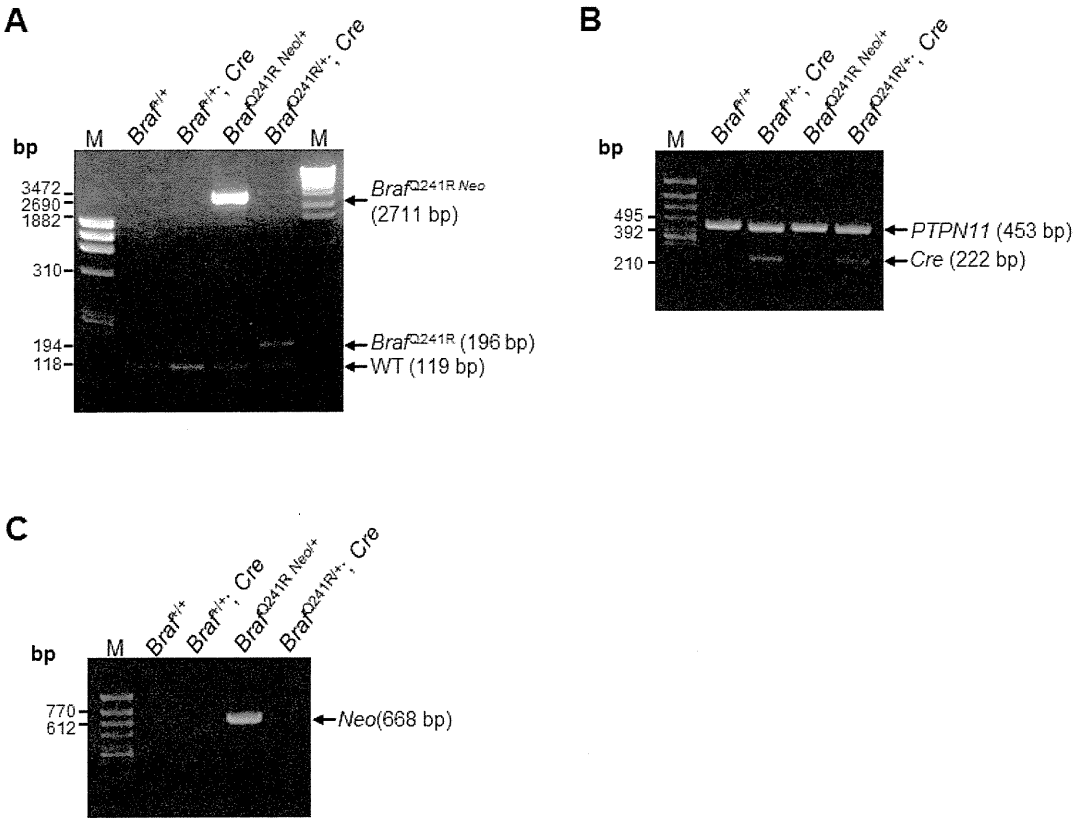

Supplementary Figure 1 PCR-based genotyping of DNA from *Braf*$^{+/+}$, *Braf*$^{+/+}$; *Cre*, *Braf*$^{Q241R\ Neo/+}$ and *Braf*$^{Q241R/+}$; *Cre* mice. (**A-C**) Genotyping of embryos was performed as described in Methods. (**A**) The result of genotyping for *Braf* gene. PCR-amplified regions are indicated by the arrows in **Fig. 1B**. (**B**) The result of genotyping for the 222-bp product from *Cre* recombinase gene. PCR amplification of a part of the *PTPN11* gene (453 bp) was used as an internal control. (**C**) Genotyping for 668-bp neomycin gene product. M, molecular mass marker.

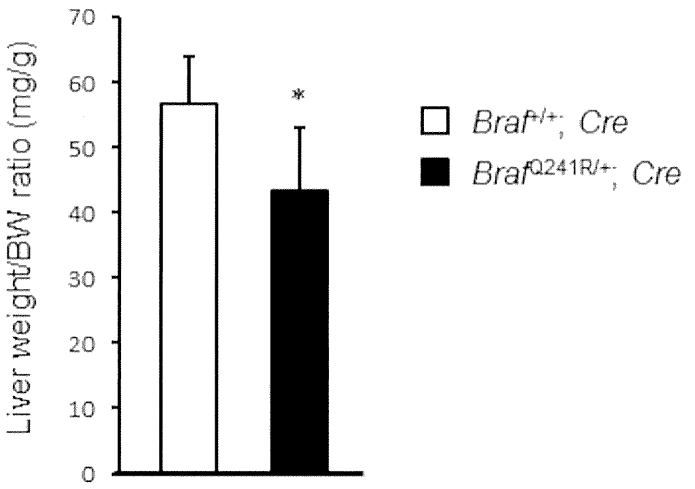

Supplementary Figure 2 Decrease of liver weight in *Braf*$^{Q241R/+}$; *Cre* embryos at E18.5. Liver weight to body weight ratios of *Braf*$^{+/+}$; *Cre* and *Braf*$^{Q241R/+}$; *Cre* embryos at E18.5. Data are the means ± S.D. (*Braf*$^{+/+}$; *Cre* (n = 7) and *Braf*$^{Q241R/+}$; *Cre* (n = 5)). *, P<0.05.